Structural Biology and Molecular Biophysics

Revealing a hidden conducting state by manipulating the intracellular domains in K_V10.1 exposes the coupling between two gating mechanisms

Reham Abdelaziz, Adam P. Tomczak, Andreas Neef, Luis A. Pardo

Oncophysiology Group. Max Planck Institute for Multidisciplinary Sciences, City Campus • Neurophysics Laboratory. Göttingen Campus Institute for Dynamics of Biological Networks

Reviewed Preprint

Published from the original preprint after peer review and assessment by eLife.

About eLife's process

Reviewed preprint posted
September 27, 2023 (this version)

Sent for peer review
August 3, 2023

Posted to bioRxiv
July 27, 2023

Abstract

The *KCNH* family of potassium channels serves relevant physiological functions in both excitable and non-excitable cells, reflected in the massive consequences of mutations or pharmacological manipulation of their function. This group of channels shares structural homology with other voltage-gated K^+ channels. Still, the mechanisms of gating in this family show significant differences with respect to the canonical electromechanical coupling in these molecules. In particular, the large intracellular domains of *KCNH* channels play a crucial role in gating that is still only partly understood. Using *KCNH1*(K_V10.1) as a model, we have characterized the behavior of a series of modified channels that the current models could not explain. With electrophysiological and biochemical methods combined with mathematical modeling, we show that the behavior of the mutants can be explained by the uncovering of an open state that is not detectable in the wild type, is accessed from deep closed states, and reflects an intermediate step along the chain of events leading to channel opening. This allowed us to study gating steps prior to opening, which, for example, explain the mechanism of gating inhibition by Ca^{2+}-Calmodulin, and generate a gating model that describes the characteristic features of *KCNH* channels gating.

eLife assessment

This study examines the role of interaction between the PAS domain and the Cyclic Nucleotide-Binding Homology Domain (CNBHD) in voltage-dependent gating of EAG channels. The authors make the extraordinary claim that they have identified a hidden open state, thus providing a window for observing early conformational transitions associated with channel gating. Although the data are intriguing, the evidence supporting the conclusions is **incomplete**, and the experimental conditions used to propose the channel gating mechanism need to be revisited. With sufficiently strong experimental support, this work could become **important** for understanding the gating mechanisms of the KCNH family and would appeal to biophysicists interested in ion channels and physiologists interested in cancer biology.

Introduction

Voltage-gated potassium channels constitute a large family of proteins that allow K^+ flow upon changes in the membrane potential. Their general architecture consists of a tetrameric complex with six transmembrane segments (S1-S6) in each subunit to form a central pore with four voltage sensors at the periphery. S1 to S4 segments constitute the sensor domain, while S5 and S6 segments and the loop between them line the pore. The mechanism of voltage-dependent gating is well understood for several subfamilies, namely those closely related to the *Drosophila Shaker* channel (*KCNA* and *KCNB*). In this subset of families, the linker between the sensor and pore domains (S4-S5 linker) acts as a mechanical lever transferring the movement of the voltage sensor to the gate at the bottom of S6 in a neighboring subunit through physical interaction (Barros et al., 2020). Such trans-subunit interaction is commonly denoted "domain swapping." In other families, gating mechanics must be different because there is no domain swapping in the transmembrane regions. Such is the case of the EAG family (*KCNH*) (Tomczak et al., 2017;Malak et al., 2019;Whicher and MacKinnon, 2019), whose members are implicated in many pathological conditions (Bauer and Schwarz, 2018;Toplak et al., 2022), which makes them attractive therapeutic targets.

In the *KCNH* channel family, sensor-to-pore coupling does not follow the conventional model; *KCNH* channels do not display domain-swapping in the transmembrane domains, the S4-S5 segment is very short and does not form a helix (Whicher and MacKinnon, 2016;Wang and MacKinnon, 2017) and voltage-dependent gating in $K_V10.1$ (Lörinczi et al., 2015) or $K_V11.1$ (de la Pena et al., 2018) occurs even when the S4-S5 linker is severed or removed. *KCNH* channels show extensive conserved intracellular domains. The eag domain in the N-terminus, formed by the PAS domain and PAS-Cap, interacts with the CNBHD (cyclic nucleotide-binding homology domain) of the neighboring subunit, which is connected to the S6 through the C-linker, see Fig. S1A). The four eag-CNBHD complexes form a ring in the intracellular side of the channel, connected to the gate via the C-linkers (Whicher and MacKinnon, 2016;Whicher and MacKinnon, 2019). Thus, there is domain-swapping within intracellular domains instead of the transmembrane segments (reviewed e.g., in (Barros et al., 2020;Codding et al., 2020)). This arrangement makes the intracellular ring an excellent candidate to participate in the gating process, as it has been demonstrated for other channels, e.g. (James and Zagotta, 2017;Codding et al., 2020;Nunez et al., 2020;Verkest et al., 2022). Indeed, gating of *KCNH* channels is affected by manipulations of either the eag domain, the CNBHD, or the interaction between them (Terlau et al., 1997;Ju and Wray, 2006;Sahoo et al., 2012;Gianulis et al., 2013;Dai and Zagotta, 2017;Dai et al., 2018;Codding and Trudeau, 2019;Malak et al., 2019;Whicher and MacKinnon, 2019;Codding et al., 2020). Furthermore, the stability of the interaction between PAS domain and C-terminus is altered by gating in KCNH2 channels (Harley et al., 2021). Recent Cryo-EM work revealed that the position of the voltage sensor in an electric field would preclude the opening of the gate (Mandala and MacKinnon, 2022). After reliving such an obstacle upon depolarization, a rotation of the intracellular ring would allow the helices at the bottom of S6 to dilate, opening the gate (Wynia-Smith et al., 2008;Thouta et al., 2014;Whicher and MacKinnon, 2016;Wang and MacKinnon, 2017;Whicher and MacKinnon, 2019). Moreover, cryo-EM data on $K_V10.2$ (which shows 76% identity with $K_V10.1$) reveals a pre-open state in which the transmembrane regions of the channel are compatible with ion permeation, but is still a non-conducting state (Tian et al., 2023).

The behavior of the intracellular ring is also subject to modulation by different factors. For example, ligand binding to the PAS domain can also modify gating (Wang et al., 2020). The association of $K_V10.1$ with calmodulin (CaM), which in the presence of Ca^{2+} efficiently inhibits the channel, adds an additional level of complexity (Schonherr et al., 2000;Whicher and MacKinnon, 2016). $K_V10.1$ has CaM binding sites at the N- and the C-termini (Ziechner et al.,

2006;Gonçalves and Stühmer, 2010). CaM presents two lobes (N- and C-lobe) that bind Ca^{2+} and a flexible helix in between. The N-lobe of CaM (Babu et al., 1985) binds to the N-site in the channel, while the C-lobe binds the C-terminal sites of an opposite subunit (Whicher and MacKinnon, 2016). This represents a cross-linking of two segments of the ring that possibly impairs its rotation and can thus be the basis of the inhibitory action of CaM through modulating the intracellular ring.

Yet, the mechanism coupling the movement of the sensor and the rotation of the ring remains unsolved. Importantly, mutations in both the intracellular N- (Whicher and MacKinnon, 2019) and C-terminal domains cause unexpected rectification (Zhao et al., 2017) or paradoxical activation by Ca-CaM instead of the normal inhibition seen in wild type (Lörinczi et al., 2016). In this study, we provide a mechanistic explanation of the hallmarks of K_V10.1 gating and define the role of the intracellular ring using a combination of electrophysiology and mutagenesis, modeling, and biochemical approaches. Channel variants with altered interaction between PASCap and CNBHD uncovered an open state in the mutants, different from the main open state in the wild type, with higher conductance. This made the transition between the voltage sensor movement and the ring rotation visible, allowing the characterization of gating steps hidden in the wild type. The novel open state can be best accessed from deep closed states (strong hyperpolarized membrane potential) and is promoted by binding of CaM, thus explaining the paradoxical effects of CaM in mutant channels. We propose a model tightly constrained by data that can explain the main differential features of K_V10.1 gating.

Results

Disrupting the interaction between PASCap and CNBHD reveals a biphasic gating behavior

The first N-terminal residues of K_V10.1 are prime candidates for the transmission of voltage sensor motion to the intracellular domain based on crystal structures and interactions inferred from mutant function. In particular, two residues at the bottom of S4 (H343 (Terlau et al., 1997) and D342 (Tomczak et al., 2017)} functionally interact with the initial N-terminus. The N-terminal PAS domain can then transmit mechanical cues to its C-terminal interaction partner CNBHD (Whicher and MacKinnon, 2016;Codding and Trudeau, 2019;Whicher and MacKinnon, 2019;Codding et al., 2020;Wang et al., 2020;Mandala and MacKinnon, 2022). To study K_V10.1 gating under perturbed intramolecular interaction, we deleted the PASCap domain (residues 2-25) and, in a more conservative approach, we examined the impact of a point mutation (E600R) reported to disrupt the PASCap-CNBHD interaction (Haitin et al., 2013). We then obtained the response of the mutants to discrete depolarizations to different potentials (-100 to +120 mV for 300ms) in *Xenopus* oocytes in the presence of 60 mM K^+ in the extracellular solution to follow deactivation behavior through tail currents.

Fig. 1A displays representative current traces of WT and the mutant channels. The threshold for activation was shifted towards hyperpolarizing values in both mutants, giving rise to inward currents at potentials that do not lead to the opening of WT channels. This is most obvious in the biphasic conductance-voltage (GV) plots (**Fig. 1B**). The kinetics of activation (**Fig. 1C**) and deactivation (**Fig 1E**) of the mutants were also clearly distinguishable from WT. To facilitate the description of the results, we classified the responses into three categories depending on the stimulus amplitude: *weak* (-90mV to -20mV), *moderate* (-10mV to +40mV), and *strong* (+50 to +120mV).

While the activation of WT currents does not accelerate dramatically with increasing depolarizations in the voltage range tested, the mutants activated much slower than the WT upon *weak* and *moderate* depolarizations, reaching activation kinetics similar to WT with *strong* ones,

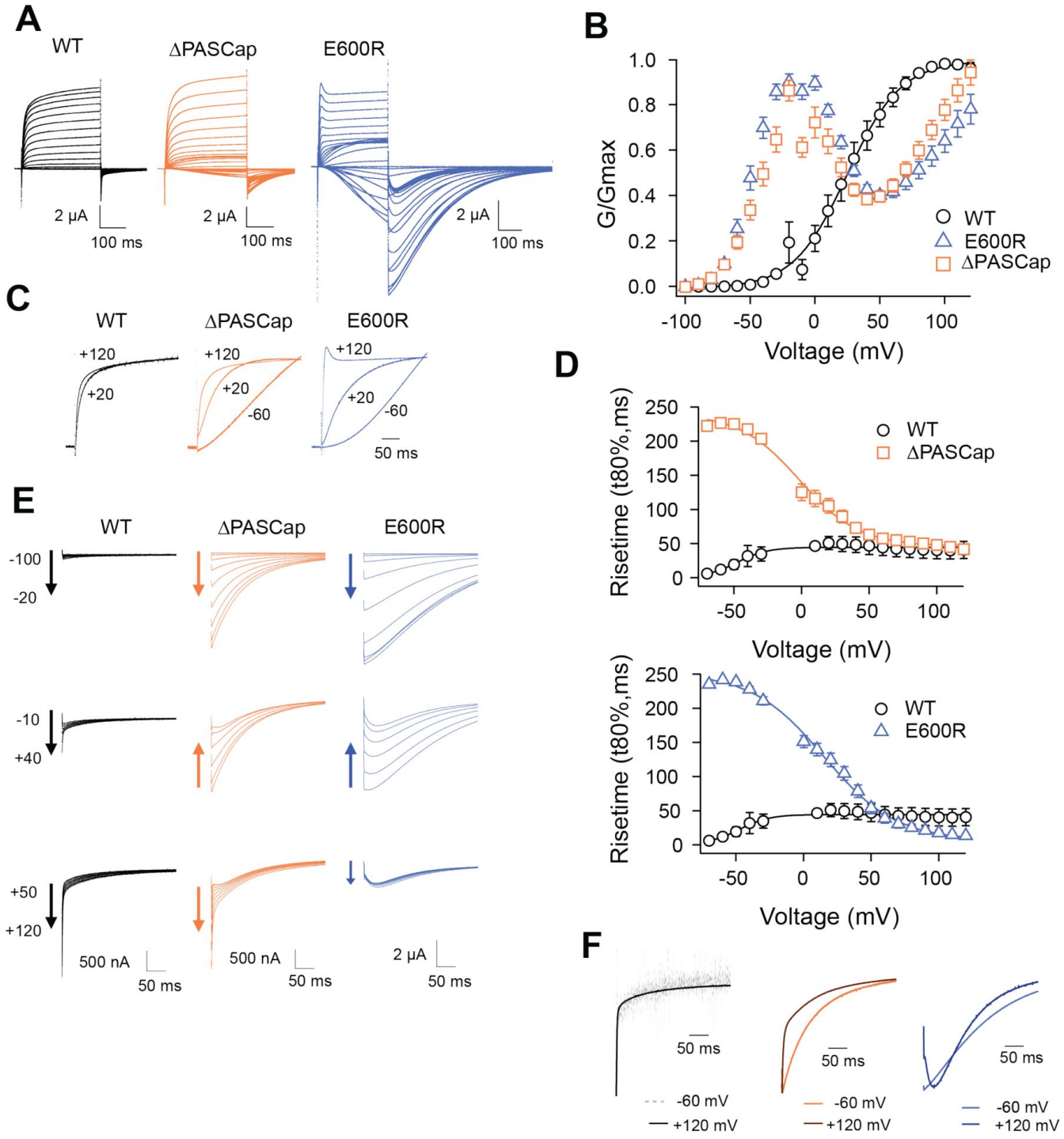

Figure 1.

Characterization of ΔPASCap and E600R mutants.

A. Raw current traces resulting from depolarizations between -100 and +120mV in WT (black), ΔPASCap (orange) and E600R (blue). **B**. GV plots corresponding to the three channel variants (colors as in A). (N: WT = 6, ΔPASCap = 7, E600R = 11; mean±SEM) **C**. Normalized traces to the indicated voltages to reveal the acceleration of activation with depolarization in the mutants. WT does not activate at -60mV type. **D**. Rise time of ΔPASCap (up) and E600R (down) as a function of voltage. The activation is much slower than in WT up to +50mV but reaches the speed of WT with stronger stimuli. **E**. Tail currents at -100 mV after depolarizations to potentials in the weak, medium, or strong range (up to down, see text for details). The arrows indicate the direction of the change in tail peak amplitude with increasing voltage. **F**. Normalized tail currents at -100 mV after depolarizations to the indicated voltages.

as can be observed in normalized traces (**Fig 1C**). To obtain a more quantitative estimation of the changes in activation velocity, we used the time required to reach 80% of the maximum current amplitude plotted against the stimulus voltage (**Fig. 1D**). ΔPASCap and E600R needed a much longer time than WT to activate at *weak* depolarizing potentials but were equally fast at membrane potentials larger than +50 mV.

The deactivation (tail) kinetics changes with increasing depolarizations were more evident and more complex than changes in activation kinetics (**Fig. 1E** and **1F**). For increasing test pulse potentials, the peak amplitude of ΔPASCap tail currents first increased progressively, then decreased at *moderate* values, and rose again after the range of *strong* depolarizations. E600R showed a similar pattern of tail amplitude, although the increase at *strong* potentials was less pronounced. Remarkably, both the tail amplitude and its decay kinetics underwent profound changes depending on the stimulus. While the kinetics of WT tail currents was the same across different potentials, showing the characteristically fast deactivation of K_V10.1, ΔPASCap deactivated slow- and monotonically at *weak* depolarizations, but a fast component started to become evident after *moderate* stimuli. The fast component dominated the process at *strong* depolarizations. For E600R, the deactivation after *weak* stimuli was also slow and accelerated after a rising phase in the *moderate* and *strong* depolarization range.

Due to the complex behavior of the tail currents, different equations would be needed to fit the tails of the various channels to extrapolate the amplitude to time zero. Hence, to calculate the conductance, we simply used the current amplitude at the end of the stimulus and divided it by the driving force calculated from the reversal potential (**Fig. 1B**). As already observed in the raw traces, the threshold for activation for both mutants was strongly shifted in the hyperpolarizing direction with respect to WT (-80mV *vs.* -20mV). Still, the most evident change was that both ΔPASCap and E600R displayed a biphasic GV in contrast to WT. *Weak* depolarizing pulses increased the conductance of both mutants until a maximum at approximately +10mV. With further depolarizations, the conductance initially declined to rise again in response to *strong* depolarizations. This finding matches the changes in amplitude of the tail currents, which, therefore, probably reflect a true change in conductance. A similar behavior had been mentioned for related (Whicher and MacKinnon, 2019) or unrelated mutations (Zhao et al., 2017) affecting the intracellular domains. However, the reasons for this phenomenon had not been investigated. We thus aimed to understand the molecular mechanisms underlying the biphasic GV.

The biphasic GV is described by two sigmoidal components corresponding to a two-step gating mechanism

One possible explanation for the biphasic behavior could be the coexistence of two separate channel populations with different kinetics, conductance, and voltage dependence. This seems unlikely because the shape of the GVs was consistent in all our recordings, as evidenced by the small error bars (**Fig. 1B**) despite the variability intrinsic to the oocyte system. Alternatively, each channel could have two open states, and the rectification observed between the two conductance components represents a transition from one state to the other. Indeed, an equation that reflects the two components and a transition between them (see Methods) described the behavior of the GV of both mutants accurately (**Fig. 2A**).

With the available structural information in mind, the two components could represent sequential access to two open states (from here on, O_1 and O_2) through two gating steps that differentially involve the sensor movement and ring rotation (Tomczak et al., 2017;Whicher and MacKinnon, 2019;Mandala and MacKinnon, 2022).

To test if the ring underlies one of the two gating steps, we tested the behavior of additional N-terminal deletions of increasing length (Δ2-10, 2-25 for ΔPASCap, and 2-135 for Δeag), expected to disrupt the ring integrity more and more. A biphasic GV was observed in all these mutants (**Fig.**

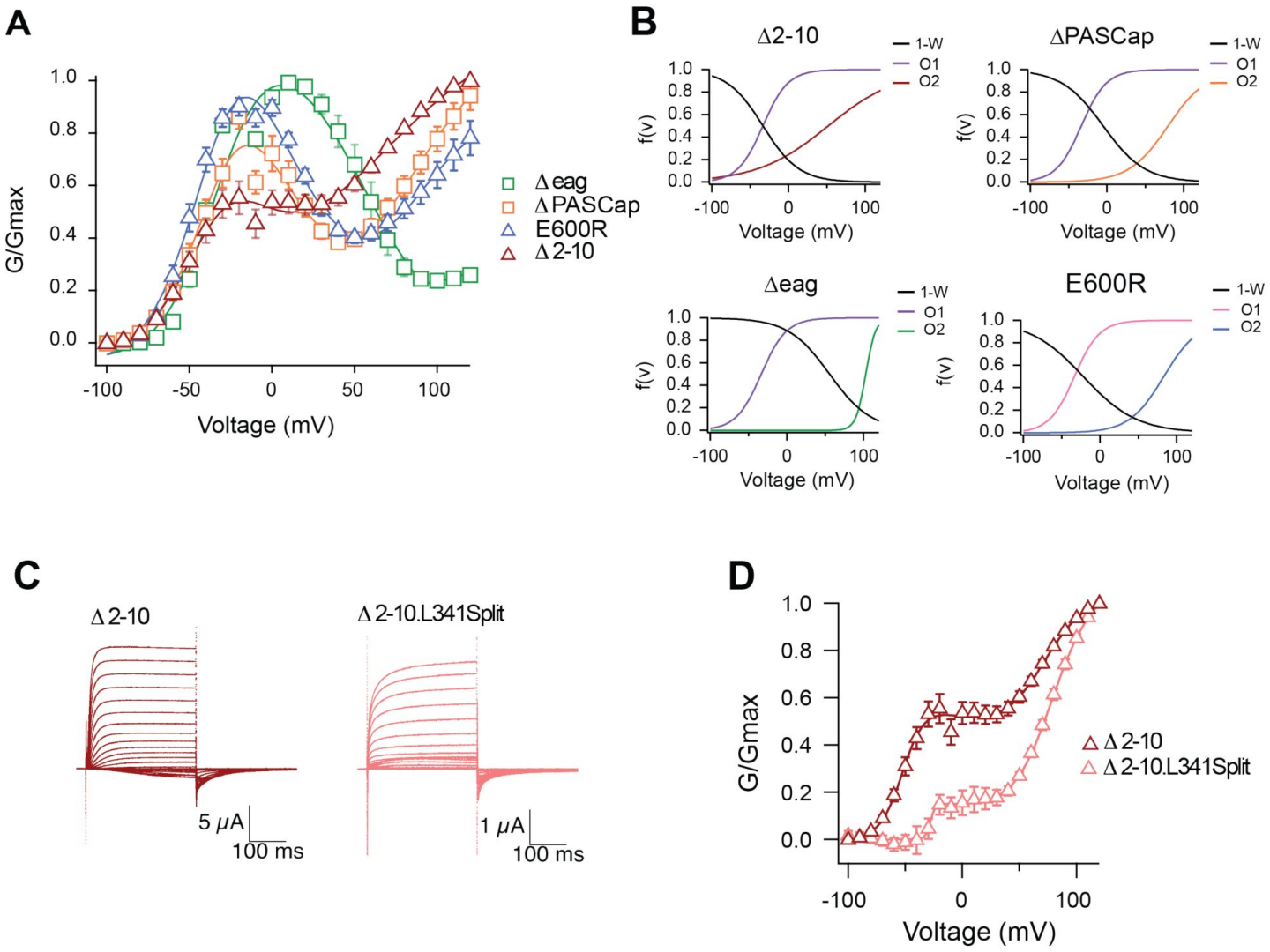

Figure 2.

The biphasic GV corresponds to two sequential events.

A. The GV of all tested mutants show biphasic behavior. (N: Δ2-10 = 6, ΔPASCap = 7, Δeag = 7, E600R = 11; mean±SEM). All are well described by ***Eq. 4*** in a global fit with fixed parameters for the first component. **B**. Distribution of the three components used for the fits as a function of voltage. **C**.A discontinuous form of Δ2-10 shows attenuated biphasic behavior. **D**. GV plots of Δ2-10 and Δ2-10.L341Split (N: Δ2-10 = 6, Δ2-10.L341Split = 5; ±SEM). Split fitted using ***Eq. 4***.

2A). The V_{half} value of the first component was very similar across mutants. In contrast, the second component showed different thresholds. We then performed a global fit using **equation 4**, where we linked the parameters of the first components (Vh_1, K_1) across mutants and allowed the parameters for the second component (Vh_2, K_2, A_2) and the transition (Vh_3, K_3) to vary (**Table S1**, **Fig. 2B**). The global fit accurately described the behavior of the GV in all mutants (**Fig. 2A**).

The result of the global fit indicates that the first component is conserved across mutants. In contrast, the second component occurs at progressively more depolarized potentials for increasingly larger N-terminal deletions. Thus, the underlying gating events can be separated into two steps: A first gating step of the voltage sensor, which affects opening without engaging the ring and leads to a non-conducting pre-open state in the WT which is conducting in our mutants, and a second gating event, operating at higher depolarizations, that involves a change in the ring.

To test this hypothesis, we compared the behavior of Δ2-10 and Δ2-10.L341Split, a channel lacking a covalent connection between the sensor and the pore domain (Tomczak et al., 2017) hence decoupling residues downstream S4 (in this case starting from 342) from the movement of the sensor. As predicted, compared to Δ2-10, Δ2-10.L341Split showed a significant reduction in the first component of the biphasic GV (**Fig. 2C**, D).

Activation of WT K_V10.1 channels (best studied for the *Drosophila* form *eag*) drastically slows down in the presence of extracellular divalent cations that bind to the voltage sensor (Silverman et al., 2000;Tang et al., 2000), e.g., Mg^{2+}, Ni^{2+}, Co^{2+}, and Mn^{2+}, but not Ca^{2+}. Strikingly, the degree of deceleration correlates with the ions' hydration enthalpy, suggesting that the ion might unbind during activation (Terlau et al., 1996). In addition, deep deactivated states are accessed with less hyperpolarization when these divalents are present. We chose to study the impact of Mg^{2+} on the kinetics and voltage dependence of activation (**Fig. 3**) in the mutant Δeag, which shows the most significant separation between the two conductance components. Mg^{2+} slowed the activation of the channel at all depolarizations, affecting entry to both open states. This result suggests that Mg^{2+} also slows the voltage sensor motion that controls access into the second open state. In addition, the voltage dependence of activation was shifted by approximately 25 mV to more depolarized voltages. This is in line with Mg^{2+} promoting access to deep deactivated states requiring stronger depolarization to exit them. Interestingly, the transition from the first to the second component of the GV plot seems unaffected by the divalent binding.

Steady-state voltage dependence and activation kinetics are consistent with two open states (O_1 and O_2) with different conductance

Thus far, our results are compatible with two different open states in the mutants. The first open state, the mutant-specific O_1, would dominate at *weak* depolarizations and deactivate slowly, with tail current decay time constants of tens of milliseconds. In contrast, mutant and WT channels would reach the second open state (O_2) at strong depolarizations and deactivate more rapidly, with a few milliseconds or less time constants. A critical test of this hypothesis is the application of more complex voltage stimuli that drive the system to a non-equilibrium state of high O_1 occupancy. This might be achieved by deactivation periods of around 10 ms, just long enough to remove most channels from O_2 but sufficiently brief to maintain the occupancy of O_1. For simplicity, we used depolarization periods of the same duration and tested whether a 300 ms series of activating and deactivating 10 ms pulses could accumulate channels in a high conductance state O_1.

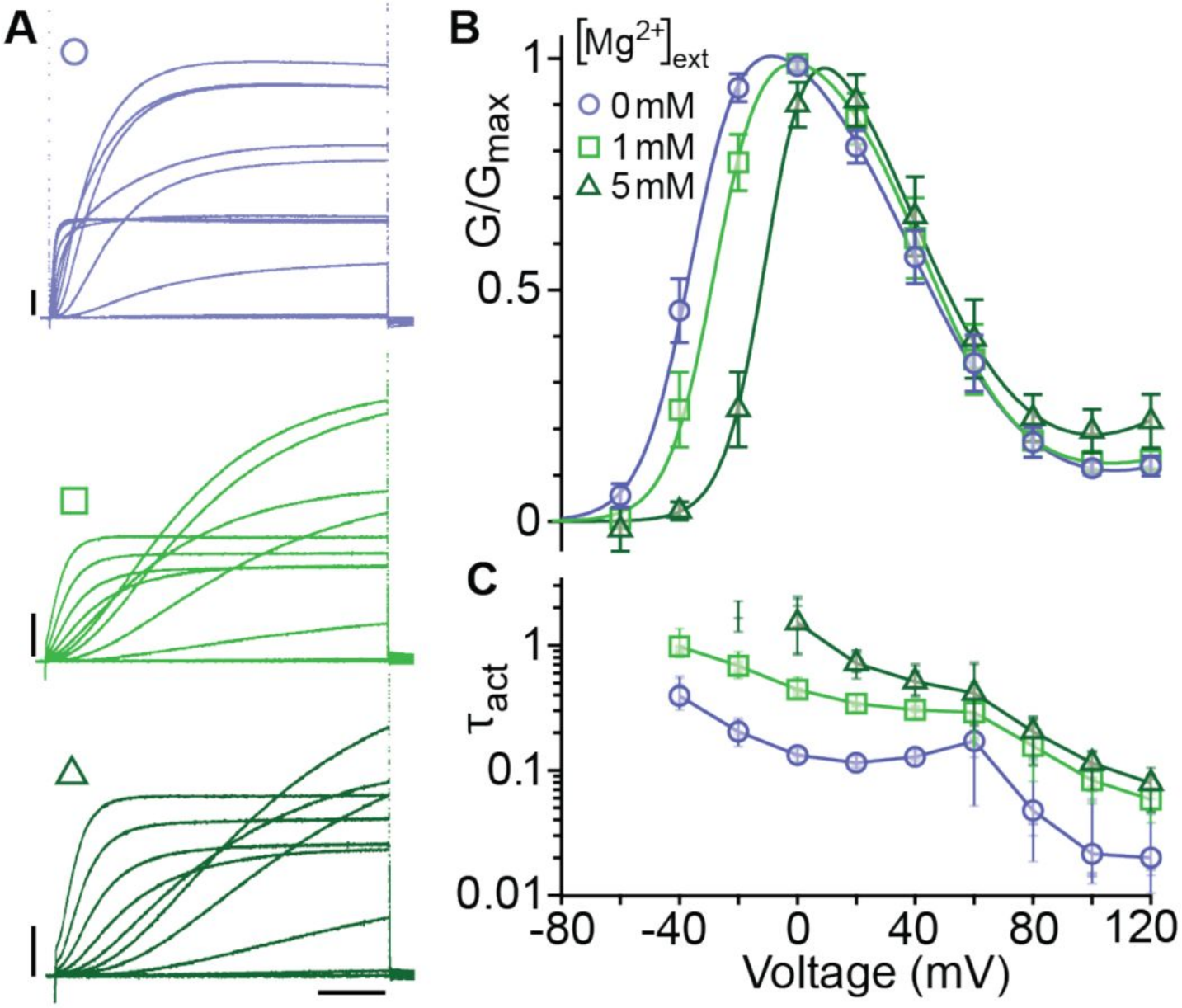

Figure 3.

Mg^{2+} induces a shift of the first component in the depolarizing direction.

A. Raw current traces from oocytes expressing Δeag channels in response to depolarizations from a holding potential of -100 mV to voltages between -100 and +120 mV in the presence of 0, 1 or 5 mM $MgCl_2$ in the external solution (legend in B). Scale bars are 1μA and 200 ms. **B**. Average GV plots (with SEM) obtained under the same conditions from n=6, 6, and 5 recordings (0, 1, and 5 mM $MgCl_2$). The V_{half} of the first component shifts from -35.8 mV in the absence of extracellular Mg^{2+} to -27.9 and -9.9 mV in 1 mM and 5 mM $MgCl_2$. **C**. Time constants of the early activation show decelerating effect of Mg^{2+}. Symbols depict averages, vertical lines the range and horizontal lines individual experiments. For voltages, where conductances or time constants could not be reasonably estimated no data are displayed.

For WT (**Fig. 4A**), alternating between -80 and +80 mV resulted in a smaller amplitude than a constant stimulus to +80 mV, just as expected for a system with a single open state and a monotonic voltage dependence of activation. What is more, the rapid deactivation of WT resulted in near-complete deactivation during every cycle.

In E600R, in contrast, the current amplitude during activating pulses increased steadily from cycle to cycle. Ultimately the current amplitude exceeds that obtained with a constant +80mV pulse (**Fig. 4A**). Because the deactivation of this mutant is much slower and occurs at more negative potentials than that of WT (see **Fig. 1** and **2B**), there was no noticeable deactivation during the -80 mV episodes. In addition, the tail current after the alternating stimuli had a larger amplitude than the one after a continuous pulse and decayed mostly as one component. All those observations are consistent with an accumulation of channels in O_1. A similar behavior was detected with ΔPASCap (**Fig. 4B**), albeit within a different voltage range, as could be predicted from the different voltage dependence of the transition between states (**Fig. 2B**). Again, alternating pulses resulted in larger current amplitudes and less complex tail current as compared to a single long pulse (**Fig. 4B**).

Deep-closed states favor access to O_1

A hallmark of $K_V10.1$ gating is the Cole-Moore shift, the change in activation kinetics in dependence on the pre-pulse potential (Cole and Moore, 1960). Hyperpolarized potentials drive the channel into deep closed states, which delays and decelerates activation (Ludwig et al., 1994; Hoshi and Armstrong, 2015). This is well described by a model with four identical, independent transitions of the voltage sensor (Schonherr et al., 1999) and is compromised by N-terminal deletions (Whicher and MacKinnon, 2019). To test the behavior of our mutants concerning this property, we applied a series of 5s-long conditioning pulses with voltages ranging from -160mV to -20mV, followed by a test pulse to +40mV in the absence of external Cl^-. The activation kinetics, quantified by the time to 80% of the maximum current, showed a strong pre-pulse dependence in WT, ΔPASCap, and E600R, with much larger rise times in both mutants (**Fig. 5B**).

In the mutants, not only activation kinetics but also current amplitude was substantially affected by hyperpolarizing pre-pulses. With respect to the -100mV pre-pulse potential, the current starting from a -160mV pre-pulse increased in ΔPASCap by a factor of 3.93 ± 0.36 and in E600R by a factor of 2.65 ± 0.54. In contrast, WT current amplitude was not significantly affected (**Fig. 5A**, 5C). Such increases in amplitude are often related to augmented channel availability due to voltage-dependent de-inactivation. Still, conventional inactivation was never detected in any mutants after repeated or prolonged depolarization. In the absence of inactivation, the prepulse-dependent current increase at +40 mV could be related to changes in the relative occupancy of the open states. We hypothesized that the higher conductance open state O_1 might be more accessible after hyperpolarization. The current decay after the peak (**Fig. 5A**), especially in ΔPASCap, also indicates a transient phenomenon. To map the voltage dependence of this effect more comprehensively, we next compared the effect of hyperpolarized pre-pulse on currents elicited at different test potentials.

We tested the effect of pre-pulse potentials (-160 and -100 mV) on IV protocols in the absence of Cl^-. Compared to a -100mV pre-pulse, -160mV clearly potentiated the first component of ΔPASCap and E600R biphasic IV (**Fig. 6A** and **6B**).

If the hyperpolarizing potentials facilitate the access to O_1 by driving the channel into deep closed states, then impairing the access to these states will reduce the component corresponding to O_1 in the GV. The mutation L322H, located in the S3-S4 linker, limits access to deep closed states in WT channels (Schonherr et al., 1999). We introduced this mutation in the context of ΔPASCap and E600R. Representative current traces obtained from $\Delta PASCap^{L322H}$ and $E600R^{L322H}$ are shown in

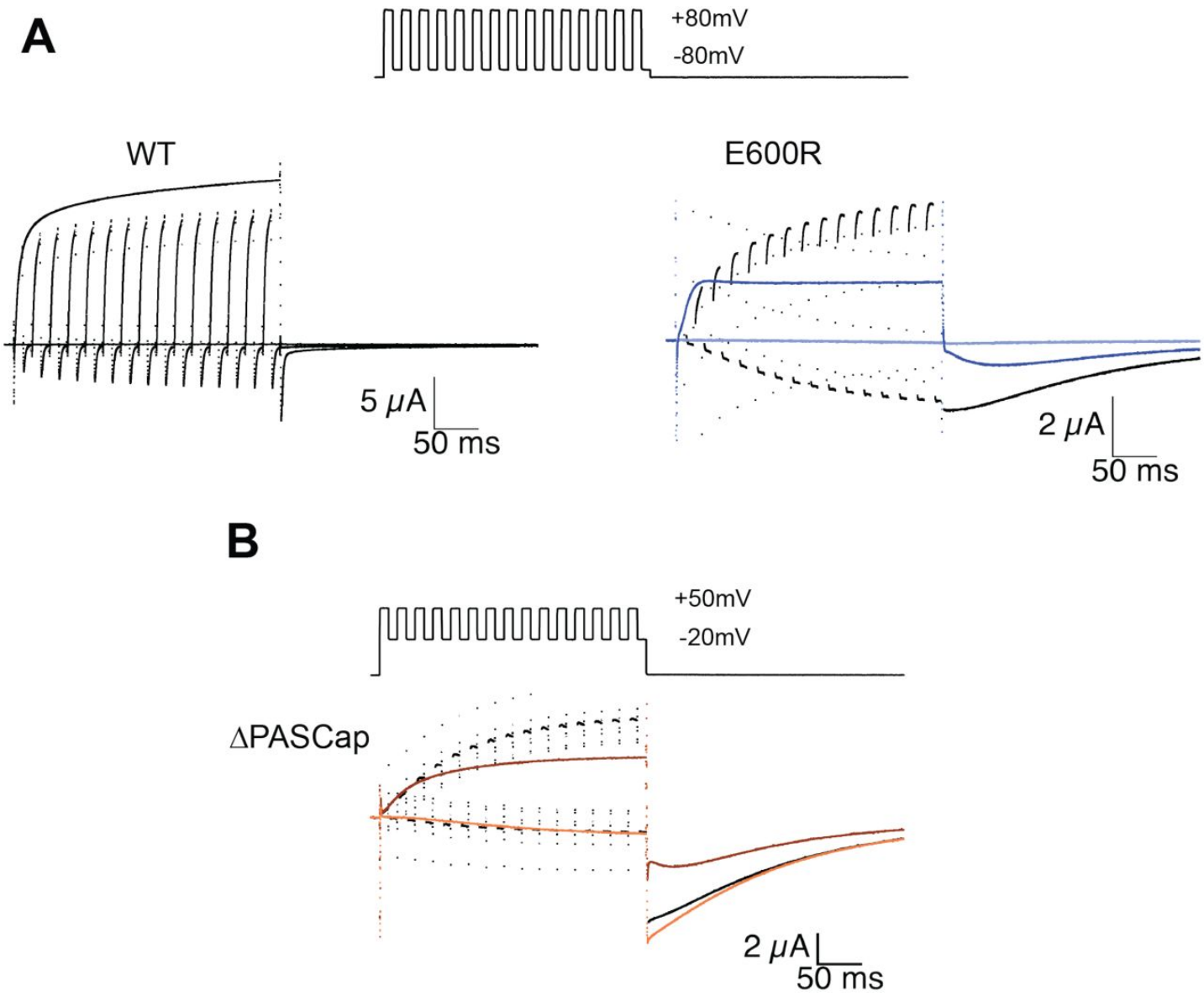

Figure 4.

Alternating stimuli reveal larger conductance for O_1.

A. Alternating potential between -80 and 80 mV in the WT results in current amplitudes that are smaller than those during a sustained stimulus (Upper left traces). In contrast, E600R gave rise to larger currents when the stimulus was intermittent and too short to allow occupancy of O_2 (upper right). **B**. The effect was qualitatively similar for ΔPASCap, which consistently gave rise to larger current upon oscillating stimuli between -20 and +50 mV than during a constant pulse to +50 mV.

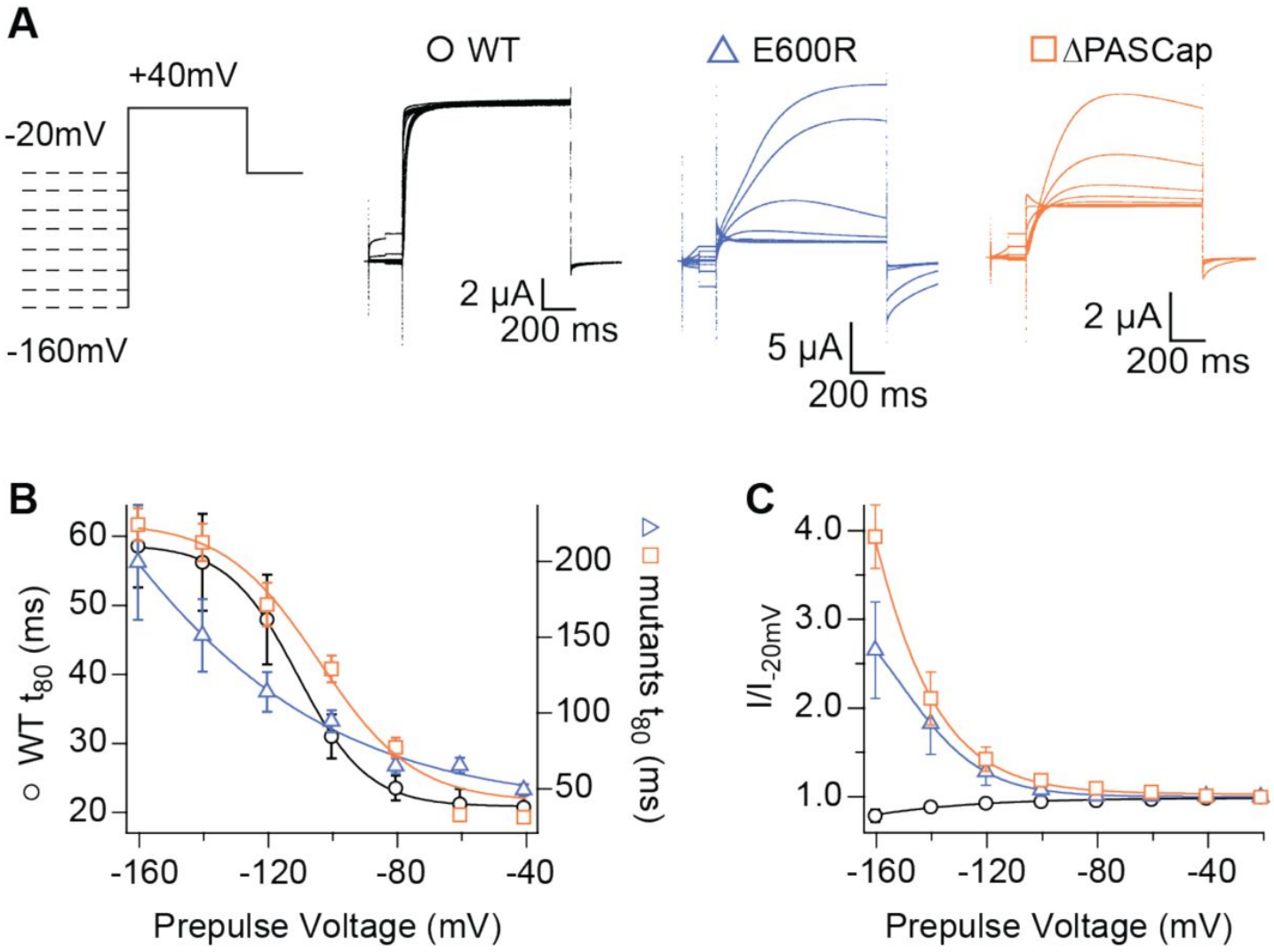

Figure 5.

Hyperpolarization promotes access to a large conductance, slowly activating open state.

A. Raw current traces in response to the stimuli depicted in the scheme. **B**. The rise time to 80% of the maximal current during the depolarizing stimulus is plotted *vs*. prepulse voltage (N: WT = 7, ΔPASCap = 9, E600R = 8; mean±SEM). Although the activation is much slower for both mutants (note the different y axis for the mutants), they retain a strong dependence on the prepulse potential. **C**. Normalized end-pulse current (I/I_{-20}) is plotted *vs*. prepulse voltage (N: WT = 10, ΔPASCap = 8, E600R = 8; mean±SEM). The amplitude of the current at +40 mV increased markedly when the holding potential was below -100 mV in the mutants, while the amplitude in WT changed only marginally.

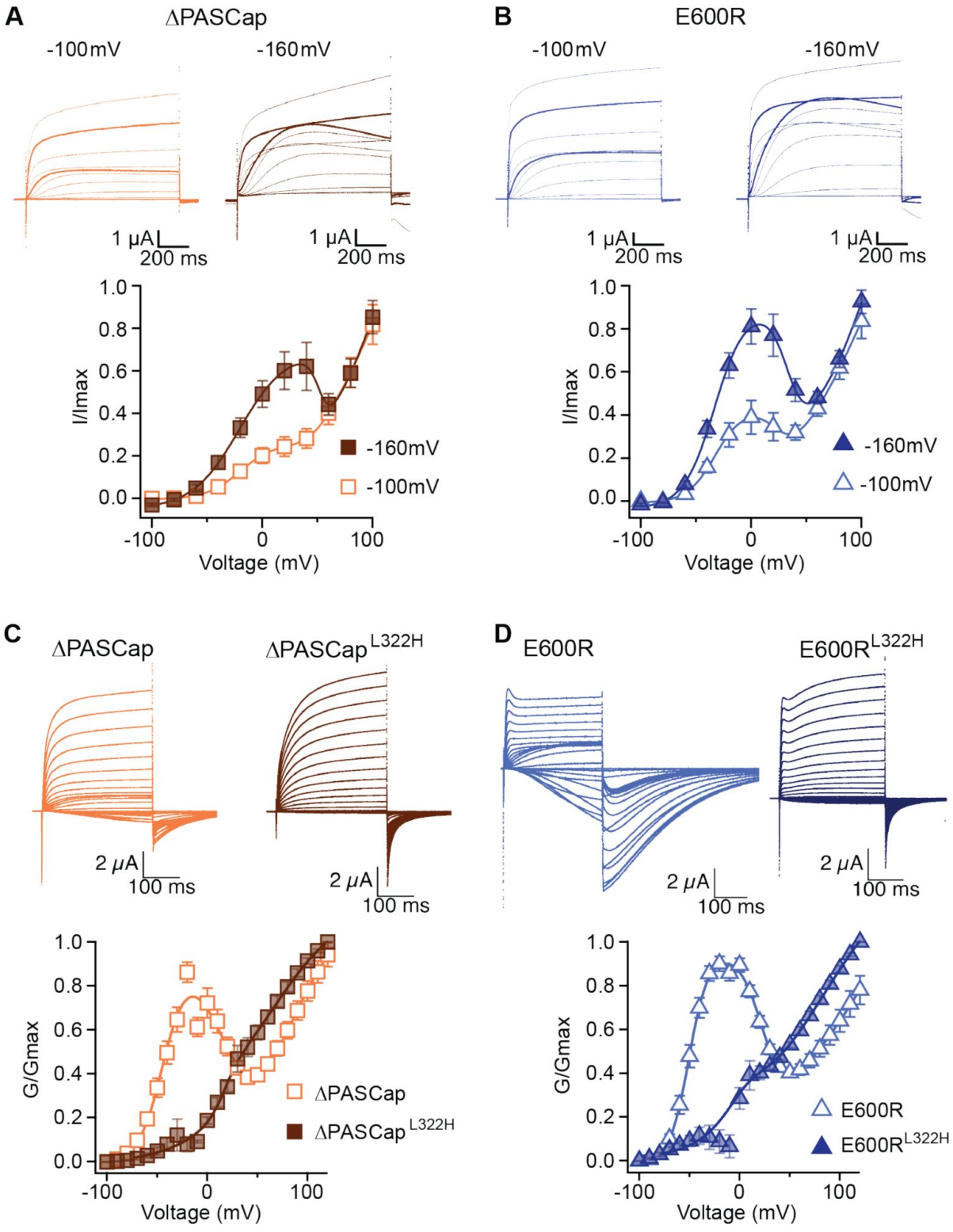

Figure 6.

Deep closed states facilitate access to O_1.

A, B. Conditioning pulses to -160 mV potentiated the first component and hence the biphasic behavior of the I/V relationships for ΔPASCap (A) and E600R (B). (N: ΔPASCap = 7, E600R = 6; mean±SEM) **C, D**. A mutation known to impair access to deep closed states (L322H) largely removes the initial phase of the GV curves for ΔPASCap (C) and E600R (D). (N: ΔPASCap = 7, $\Delta PASCap^{L322H}$ = 6, E600R = 11, $E600R^{L322H}$= 7; mean±SEM).

Fig. 6 C and D. Both mutants showed drastic attenuation in the first component of the biphasic GV compared to the parental channels. The tail currents of $\Delta PASCap^{L322H}$ and $E600R^{L322H}$ did not show rectification. They presented homogenous kinetics at all potentials, indicating that reducing the access to deep closed states also reduces the occupancy of O_1.

Ca^{2+} Calmodulin stabilizes O_1

The available Cryo-EM structure shows $K_V10.1$ in a complex with Ca^{2+}-CaM. It is well established that the binding of a single Ca^{2+}-CaM inhibits the current through WT channels (Schonherr et al., 2000; Ziechner et al., 2006). In stark contrast, increasing intracellular Ca^{2+} has been reported to potentiate ΔPASCap and E600R current amplitudes (Lörinczi et al., 2016). This seemingly paradoxical behavior of mutants could be explained by the differential effects of Ca^{2+}-CaM binding on the availability of the two open states. The observations in WT and mutants would be consistent, with Ca^{2+} binding restricting access to the WT-like open state O_2 while facilitating access to the higher conductance state O_1 which is not visible in WT channels. Therefore, we predicted that Ca^{2+}-CaM would potentiate the first component of the biphasic IV in the mutants.

To test this, we induced a rise in cytosolic Ca^{2+} using the ionophore ionomycin and inducing release from the stores with thapsigargin (both 5μM) (Lörinczi et al., 2016). Because changes in intracellular Ca^{2+} are very dynamic (see **Supp. 1 to Fig. 7**) and our protocols with discrete voltage pulses require a long time to complete, we used a 5s voltage ramp from -120 to +100mV repeated every 30s for 300s. The currents were recorded in Cl^--free extracellular solution to avoid confounding effects of the endogenous Ca^{2+}-dependent Cl^- channels. The results of representative experiments on ΔPASCap and E600R are shown in the upper left panels of **Fig. 7A and B**, respectively. 60s after ionomycin/thapsigargin application, a marked potentiation of the current amplitude was observed, and the response to the ramp became linear. The current amplitude declined over the following 300s, and the biphasic IV characteristics partly recovered. The speed and extent of recovery were higher for ΔPASCap than E600R; after 150s, 39.84± 6.35% recovery for ΔPASCap, while 11.84±3.07% recovered for E600R. This recovery time course agrees with the results obtained by Lörinzi et al. for constant pulses (Lörinczi et al., 2016). The magnitude of potentiation and change in IV shape was homogeneous enough among oocytes to allow averaging of the normalized current in all experiments (**Fig. 7A and B**, lower panel). The changes in slope can be easily observed in the corresponding first derivative of the normalized IV as a function of voltage shown in **Supp. 2 to Fig. 7**.

The changes in amplitude and kinetics in response to rising intracellular Ca^{2+} support our hypothesis that Ca^{2+}-CaM stabilizes O_1, possibly by driving the channels to deep closed states (**Figs. 5** and **6**). We, therefore, predicted that forcing the channels to deep closed states using Ca^{2+}-CaM could restore access to O_1 in $\Delta PASCap^{L322H}$ and $E600R^{L322H}$. This was tested with the approach described above, increasing intracellular Ca^{2+} while recording a repeated ramp protocol in $\Delta PASCap^{L322H}$ and $E600R^{L322H}$. As seen in the representative traces in the upper right panels in **Fig. 7A and B**, we observed a notable increase in current 60 s after Ca^{2+} rise, limited to *moderate* potentials, and resembling the first phase of the ramps in the parental mutants. For both mutants, the IV returned to a linear shape after 300s. Consistent with the observations for ΔPASCap and E600R, $\Delta PASCap^{L322H}$ exhibited faster recovery than $E600R^{L322H}$. Traces normalized to the maximum current and averaged are shown in **Fig. 7A and B** (lower panel). The respective first derivatives are shown in **Supp. 3 to Fig. 7**.

To further explore the role of CaM, we introduced mutations to preclude CaM binding at the N-terminal (F151N L154N) and C-terminal (F714S F717S) binding sites. We tested the behavior of these mutants (termed BDN and BDC2) in the context of ΔPASCap and E600R constructs (**Fig 7C and D**) under conditions of basal intracellular Ca^{2+} concentration. $\Delta PASCap^{BDN}$ showed a GV relationship like ΔPASCap. In contrast, $\Delta PASCap^{BDC2}$ lost its biphasic behavior. In the case of E600R, mutation of the C-terminal binding site ($E600R^{BDC2}$) showed attenuation of the first

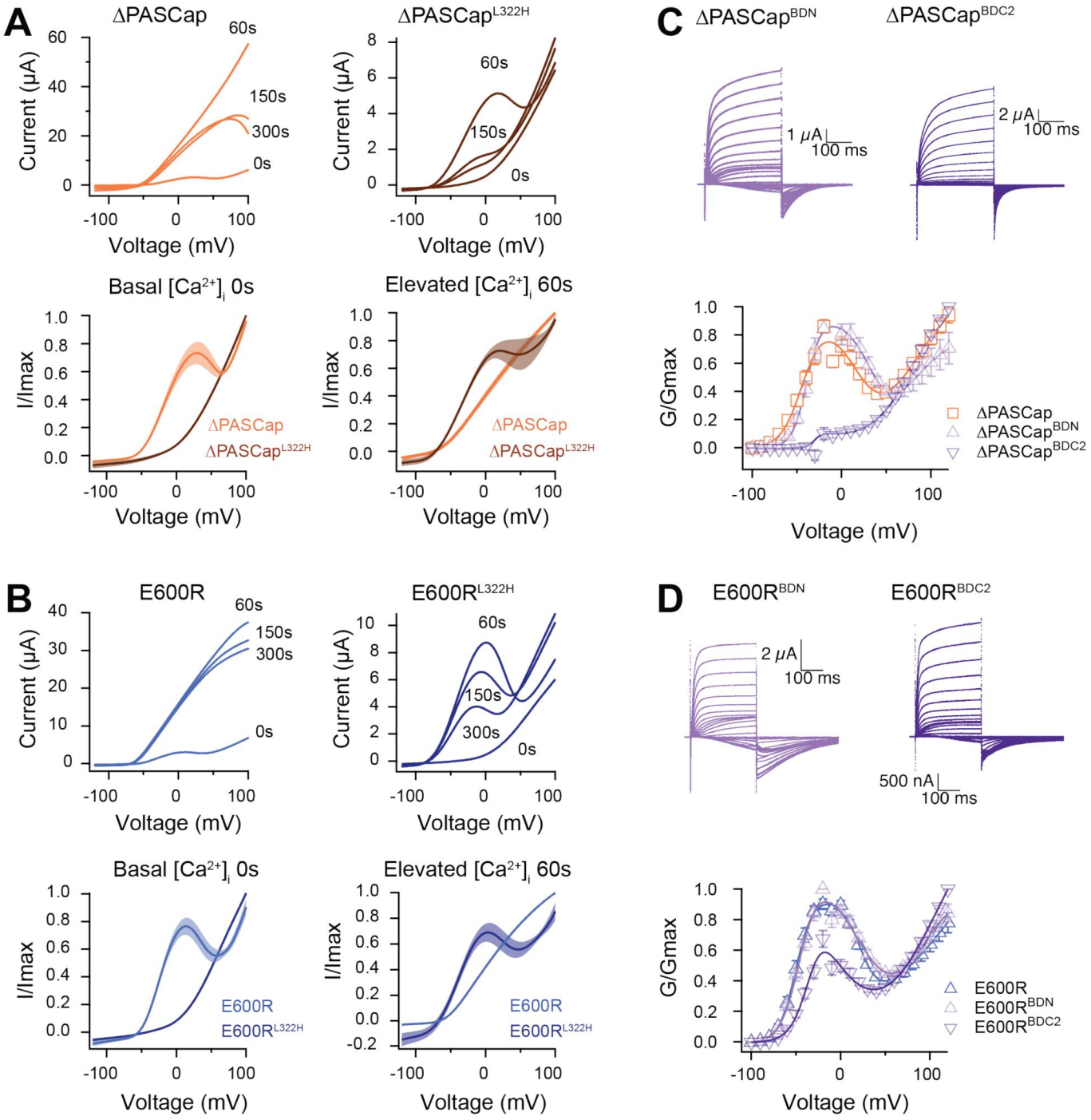

Figure 7.

CaM stabilizes O_1.

A. A transient rise in intracellular Ca^{2+} increases ΔPASCap current amplitude (in the absence of external chloride) and the IV relationship becomes linear (upper left traces). The lower traces represent the average normalized response comparing 0 and 60s. (ΔPASCap, light trace, N = 8, $\Delta PASCap^{L322H}$, dark trace, N= 5; the shadowed area indicates SEM). Right side traces: The same treatment in a channel carrying a mutation (L322H) reducing access to deep closed states results in the appearance of a biphasic IV upon Ca^{2+} rise. **B**. E600R behavior is comparable to ΔPASCap. Average normalized traces (E600R, light trace, N = 10; $E600R^{L322H}$, dark trace, N = 11; the shadowed area indicates SEM) are represented in the lower panel. **C**. Mutation of the C-terminal CaM binding domain (BDC2) in ΔPASCap reduces strongly the first component of the biphasic GV, while deletion of the N-terminal binding site (BDN) did not have any effect (N: ΔPASCap = 7, $\Delta PASCap^{BDN}$ = 7, $\Delta PASCap^{BDC2}$ = 7; mean ± SEM). **D**. The reduction of the first component in E600R when the C-terminal CaM binding site is mutated is also present but less intense. (N: E600R = 11, $E600R^{BDN}$ = 9, $E600R^{BDC2}$ = 11; mean±SEM)

component of the GV, although not complete. The attenuation of the first component when binding of CaM is disrupted supports our hypothesis that Ca^{2+}CaM stabilizes O_1. The significance of CaM for the mutants seems different. CaM might be crucial for stabilizing O_1 in ΔPASCap, while less critical in E600R.

These results opened the possibility that the biphasic behavior is due to two coexisting populations of channels, depending on CaM binding at rest. We considered this possibility but we find it is unlikely, because: i) the behavior of the mutants is very homogeneous among oocytes, in which resting Ca^{2+} is very variable; it can be as high as 400 nM (Busa and Nuccitelli, 1985), although ten times lower concentrations have also been reported (Parker et al., 1996) and ii) two independent populations of channels would not explain the rectification or the voltage-dependent transitions during short repeated alternating stimuli.

Still, it was possible that CaM is permanently bound to the channel and participates in the gating machinery while only inhibiting the current when bound to Ca^{2+}. Although the available literature would not be compatible with this hypothesis (Schonherr et al., 2000;Ziechner et al., 2006), we estimated the fraction of channels (WT or mutant) bound to CaM as a function of free Ca^{2+} concentration. We co-expressed Myc-tagged CaM and K_V10.1, extracted the proteins in different Ca^{2+} concentrations (see Methods), and pulled down the complex through the Myc-tag of CaM. Under these conditions, we could consistently detect a fraction of channels bound to CaM already in 50 and 100 nM Ca^{2+}, which increased dramatically in 0.5 and 1 μM, compatible with previous reports, suggesting that, at basal Ca^{2+}, only a small and variable fraction of channels are bound to CaM both in the WT and in the mutants (**Supp. 4 to Fig. 7**). The fraction of channels bound to CaM at basal Ca^{2+}, regardless of their stoichiometry (in the range of 4% in 100 nM, even if only one CaM is needed per channel tetramer), is insufficient to explain the prominent and proportionally constant first component observed in the mutants.

In summary, our results strongly suggest that Ca^{2+}-CaM stabilizes O_1, possibly by driving the channel to deep closed states.

A two-layer Markov model recapitulates the kinetic features of ΔPASCap

So far, our experimental results suggest that an additional open state exists in K_V10.1 mutants with a compromised intramolecular coupling. This hypothesis can explain the biphasic GV curves, the tail currents' complex shape (**Fig. 1** and **2**), the current increase following brief hyperpolarizations (**Fig. 4**), and even the paradoxical current increase under rising intracellular calcium concentrations (**Fig. 7** and its supporting figures). However, in each case, there might be alternative explanations, such as two separate channel-populations with different properties, or voltage dependent de-inactivation. The ultimate test for the hypothesis is the construction of a single model that consistently and quantitatively captures all these unusual characteristics.

We first tested whether simple addition of a second open state to the standard model of K_V10.1 activation (Schonherr et al., 1999), could replicate the experiments. However, none of these simple models could reproduce the pre-pulse dependence of entering O_1. Next, we introduced not only an additional open state, but also an additional gating step that is orthogonal to the standard model's transitions and might be related to a transition of the gating ring. This model successfully captured all the experimental observations (**Figure 8** and supporting figures).

The standard model for K_V10.1 gating comprises two gating steps for each of the four subunits' voltage sensors. The first step unfolds in the hyperpolarized voltage range and forms the basis of the Cole-Moore shift, which is characteristic for K_V10.1 channel gating. The second, faster step readies the channel for opening, and once it is performed in all subunits, a conducting state can be reached (see also (Mandala and MacKinnon, 2022)). While this model captures the key features

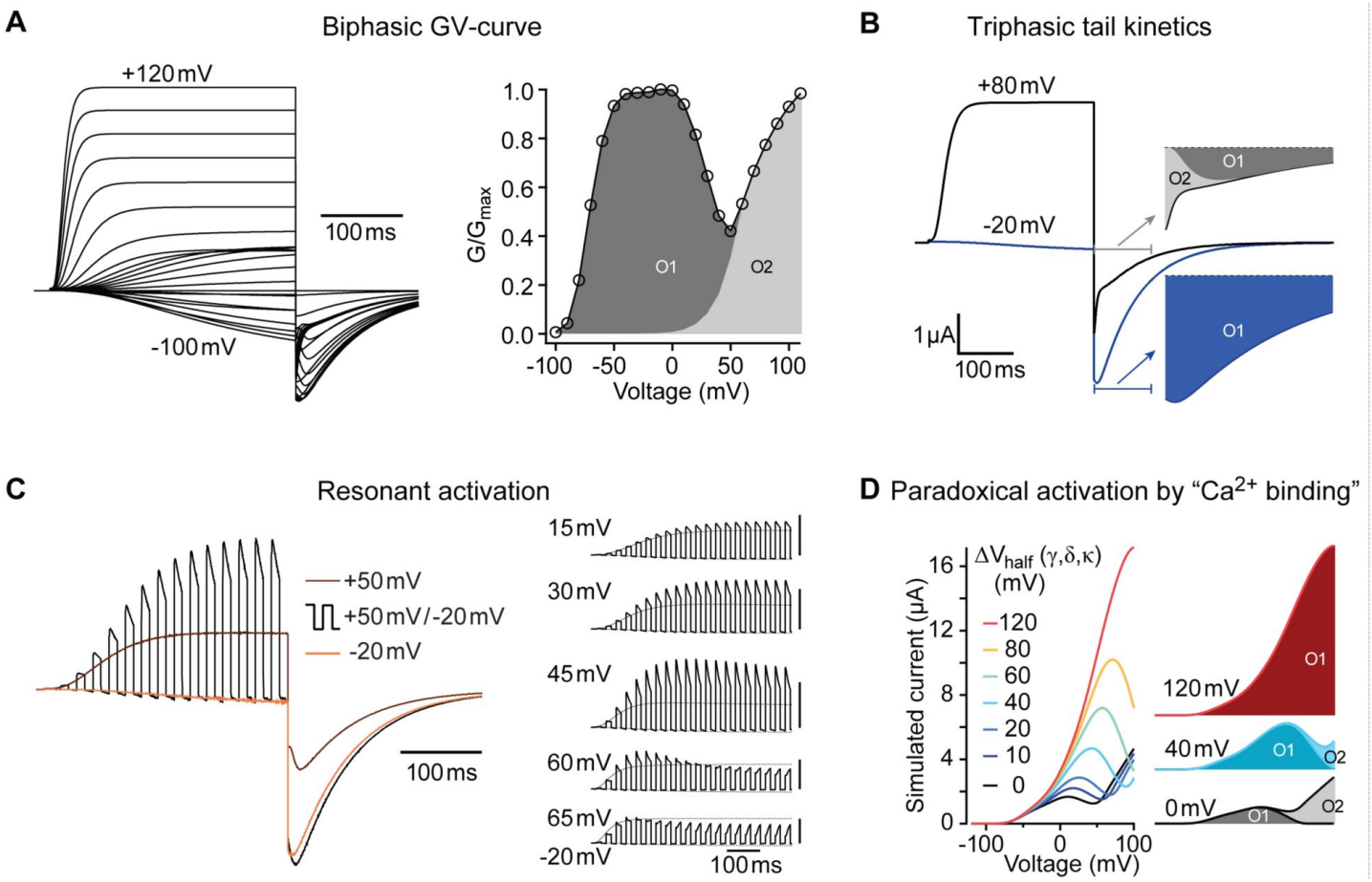

Figure 8.

A single model can reproduce all experimental observations.

A. In response to an I-V-protocol (**Fig. 1A**), the model displays biphasic activation, more clearly represented in the derived G-V curve (right, compare to **Fig. 1B**). The filled area indicates the contributions of the two open states. The tail-currents show a complex dependence on test-pulse voltage and time. **B**. Two traces from A, shown with longer repolarization. The first 100 ms of the tail currents are displayed on an extended timescale. The colored areas indicate the contributions of the two open states. After weak depolarization to -20mV, the tail-currents originate almost entirely from the mutant-specific open state O_1 (blue area). After strong depolarization, O_2 mediated currents initially dominate (light grey). The early, rapid decrease in current amplitude results from closure of O_2. During a delay phase, increasing current through an increasingly populated O_1 compensate for this closure, until eventually O_1 (dark grey) also closes, but with a much slower kinetics. **C**. In response to 10 ms pulses alternating between -20 and +50 mV, the model shows currents that exceed the currents obtained with constant pulses to +50 mV (compare **Fig. 4** B). Relating the currents during the positive and negative pulses to the concurrent currents elicited by the two constant pulses (brown and orange), the ratio lies by about 1.6 for the period starting 200 ms after the pulse onset. This excess current depends sensitively on the duration and voltage of the two pulse components. The right series of simulations displays the results for 15 ms pulses to -20 mV, alternating with 15 ms pulses to voltages from 15mV to 65 mV. The corresponding responses to the constant pulses are displayed with thin dotted lines. To facilitate perception of the excess current, the five groups of traces are scaled individually, so that the peak amplitude of the dotted response elicited by the stronger depolarizations is displayed at equal size throughout. The vertical scalebars correspond to the same absolute current. From top to bottom, the excess current ratios at 200 ms changes are 1.05, 1.38, 1.74, 1.46, and 1.16. **D**. The binding of Ca^{2+}-CaM is implemented through change in the activation energy, corresponding to a shift in the equilibrium voltage of the gating transitions. The decomposition of the current into the individual open states' contribution shows that for increasing voltage shifts – representing high $[Ca^{2+}]_i$ – the mutant-specific O_1 closes later into the ramp, until eventually all current is carried by O_1.

of WT activation, we had to extend it to account for the features of mutant gating. Throughout the model development and tuning, we focused on the experiments performed with the ΔPASCap mutant. However, a limited number of tests with other parameters showed that experimental findings with E600R can also be matched.

In a first step, we attempted a minimal model extension by attaching an additional open state to some closed state of the standard model. None of the resulting models could replicate all findings. Such a model could not replicate the multi-phasic tail currents, the pre-pulse dependence and the delayed opening under any choice of attachment site and rate voltage dependence. We came to this conclusion in two steps. First, we could exclude many possible attachment sites because the attachment site must be sufficiently far away from the conventional open state. Otherwise, the transition from "O_1 preferred" to "O_2 preferred" is very gradual and never produces the biphasic GV curves. Second, we found that the first gating transition in the standard model (left to right) can either produce a sigmoidal current onset or bias the model for occupancy of state O_1 over O_2. However, in the latter case, opening occurs without sigmoidal onset. Waveforms such as the dark orange trace in **figure 5** A, in response to a -160 mV pre-pulse and a 20mV test pulse require both: a bias towards O_1 and a sigmoidal onset. We found that this can only be accounted for by introducing a third gating step, which is orthogonal to the two transitions in the standard model. Without *a priori* information about the new states introduced in this way, we decided to simply add a copy of the standard model as an additional layer, an "upper floor". Crossing from ground floor to upper floor was made possible for any state. From a structural view, this newly added transition might be related to a reconfiguration of the gating ring. Considerations as given above lead us to attach the mutant-specific O_1 to the basal level, and the conventional O_2 to the upper level. To explain the experiments, O_1 had to be accessible to states on the right of the ground floor, and not too far towards the bottom. Eventually, we decided to attach O_1 only to the state that corresponds to completion of the first gating step in all for subunits, but no other gating step, neither the second voltage-sensor transition, nor the gating ring transition. In contrast, to enter O_2, all subunits must complete both voltage sensor transitions and also the collective gating ring transition.

It should be noted that the model structure presented here is not the only one we found to be able to reproduce the data, but it is amongst the simplest that could. We also tested models in which the upper floor was only accessible from a subset of states, and models with O_1 attached to more than a single closed state or even multiple O_1 states with varying conductances. While those more complex models offered a gradual improvement matching experimental traces, they showed no striking advantages over the more symmetric and parsimonious model presented here.

We have extensively tested variants with this symmetric structure, with a broken symmetry in the gating kinetics. In these models, the conventional gating steps (left – right, top – bottom) differed between the ground floor and the newly introduced top floor states, e.g. by introduction of factors to the α, β, γ, δ values. Under these conditions, local balance was achieved by corresponding inverse factors to the local κ and λ.

Given the large number of model parameters (41+absolute conductance), it might be surprising that the parameters can be constrained. However, the wide range of voltage protocols and the concurrent matching of depolarization and repolarization responses tightly constrains several rate ratios at different voltages and thereby ultimately all parameters. Because the model does never fit all experiments very well, a global fit proved extremely hard to balance and we decided to explore the parameter space manually, based on the time constants and rate ratios we could discern from the experiments.

The resulting model was implemented in Igor Pro. The states and transitions were defined as depicted in Fig. S8-1. For the voltage dependent transition rates, we chose a sigmoidal functional form (Eq.1).

$$x = x_0 + \frac{A_x}{1+\exp\left(\left(V_m - V_x^h\right)\cdot k_x\right)} \qquad \text{Eq. 1}$$

where x stands one of the rates α, β, γ, δ, that govern transitions in the first and second dimension of the model, which we attribute to two sequential steps of voltage sensor displacement. The rates η and θ of opening and closing of the mutant-specific open state O_1 also follow this functional form, as does the rate λ, governing the return from the upper layer. The rate κ of entering the upper layer is the sum of two components, $\kappa_{all} = \kappa_l + \kappa_r$, which again follow the same functional form. The opening and closing rates of the second open state O_2, ε and ζ, are constants.

The parameters used for the simulation are shown in **Table S2**. The model defined by the structure in figure **Supp. 1 to Fig. 8** and the voltage dependent rates in **table S2** jointly define the model that produces all results in **Fig. 8** and its supplementary figures. The only modification is done to capture the effect of Ca^{2+}-CaM-binding. If the binding influences the interaction between the intracellular modules that stabilize different configurations of the gating ring, e.g. BDC2, CNBHD, BDC1, PASCap, then the free energy of these states will change upon Ca^{2+}-CaM binding. Consequently, the free energy difference between the states and thereby the apparent voltage sensitivity of the transitions will change too. Hence, we represented the effect of different degrees of Ca^{2+}-CaM binding as different voltage shifts in λ, κ_L, γ, as indicated in **figure 8D** and **Supp. 4 to Fig. 8**.

While the Markov model describes the time and voltage dependence of state occupancies, the experimental observable is current. From the model, current was obtained by application of the GHK flux equation (**equation 5**) for both open states. The ratio between the conductances of the two opens states was adjusted to match experiments, in particular the pre-pulse-dependent activation: g_{O1}/g_{O2}=6.5.

To test the model, we focused on the most conspicuous kinetics features observed with ΔPASCap. The first feature was the tail kinetics. In contrast to the slow monophasic deactivation observed in response to *weak* depolarizing pulses (-20mV), triphasic tail kinetics was detected in response to *strong* depolarizing pulses (+80mV) (**Fig. 8B**; **Supp. 2 to Fig. 8**). The model could replicate the slow deactivation after *weak* depolarizations, fast after *strong* depolarizations, and mixed kinetics on *moderate* stimuli.

The model also reproduces the effect of a hyperpolarizing pulse on different test potentials. As described (**Fig. 6**), O_1 is preferentially accessed from deep closed states, which correspond to states in the lower layer in the model. It is plausible that a hyperpolarizing pre-pulse (-160mV), drives the channel to occupy the deep closed states (lower layer), while a pre-pulse of –100mV distributes the channel between both layers. We, therefore, adjusted the parameters accordingly (**Table S2**) and simulated the current trace (**Supp. 2 to Fig. 8**) We focused on a test pulse that represents *moderate* depolarizations (+20mV), and compared it to a *strong* depolarizing pulse (+80mV). Like in the experiment, -160mV potentiates the current at +20mV, without impacting the current at +80mV (**Supplement 2 to Fig. 8, A**). This does not happen with -100mV pre-pulse (**Supp. 2 to Fig. 8, B**).

The model also recapitulates the behavior of ΔPASCap during repeated short stimuli between -20 and +50 mV. The amplitude of the intermittent stimuli is larger than that of a sustained stimulus to the same potential. It also reproduces the relative size and the kinetics of the tail current (**Fig. 8C**.; **Supp. 4 to Fig. 8**). The effect of a rise in Ca^{2+} can be reproduced if the voltage

dependence of the rate constants for transitions between the two layers are shifted to hyperpolarized potentials, increasing the probability of states in the "lower" layer and, therefore, of the access to O_1 (**Fig. 8D**; **Supp. 5 to Fig. 8**).

To describe the behavior of $K_V10.1$ WT, we only needed to remove the access to O_1 and shift the parameters of the rotation of the ring in the hyperpolarizing direction to reflect the more stable structure resulting from intact interactions among intracellular domains and between these and the core of the channel. The model recapitulated the change in kinetics depending on the pre-pulse potential.

Discussion

The wide diversity of electrical responses in cells relies greatly on subtle differences in the behavior of voltage-gated channels. Despite the many relevant advances in the knowledge of the structure of ion channels, the correlation between the structures and the functional determinants of channel behavior is incompletely understood. In this study, we have combined biophysical, biochemical, and mathematical approaches to understand the complex gating behavior of $K_V10.1$ potassium channels, which is the basis of a group of diseases with devastating consequences (e.g. (Toplak et al., 2022;Tian et al., 2023)).

In *KCNH* channels, intracellular domains contribute to gating by forming an intracellular ring that rotates in response to depolarizing stimuli (Mandala and MacKinnon, 2022). We have studied a series of mutant channels where the integrity of the intracellular ring is compromised by either deletions or point mutations. In all the mutants, the G-V relationship shows a biphasic behavior with evident inward rectification at intermediate depolarizations and a complex deactivation with kinetics also dependent on the stimulus potential (**Fig. 1**). Our observations can be explained by the coexistence of two different open states, one of which corresponds to the stable open state observed in WT (O_2), while the other one (O_1) is made visible as a result of the modification of the intracellular gating ring. We hypothesize that O_1 corresponds in the WT to the "non-conducting state 2" identified in the closely related $K_V10.2$ channel by cryo-EM (Tian et al., 2023), in which flipping of Y460 (Y464 in $K_V10.1$) renders a hydrophobic constriction wider than 8 Å, enough to allow K^+ flow, but still corresponds to a non-conducting state. The absence of an intact intracellular ring that would preclude ionic flow in the WT would explain the permeability of this state in the mutants.

Coexistence of two independent channel populations with different gating properties could be an alternative explanation for the observed behavior. Still, it is very unlikely that two such populations would be expressed at the same ratio in all oocytes, given the variability of the system, and the behavior of each of the mutants was highly reproducible among oocytes obtained from different frogs and time points.

The atypical open state O_1 allows the study of intermediate steps between the two major gating events, VSD displacement and ring rotation. Upon intermediate depolarization, the channels would access the open states sequentially, while O_2 is predominant on strong depolarizing steps and O_1 upon mild stimuli. The analysis of the GV of the mutants using global parameters (**Fig. 2**) revealed that they all share the component responding to mild depolarizations (O_1) and only the second component (O_2) and (probably most importantly) the transition between components depends on the particular mutant studied. The larger the deletion in the intracellular ring is, the stronger the shift in the voltage dependence of the second component. Importantly, this observation is incompatible with two independent populations of channels. Since the two gating steps are sequential (Mandala and MacKinnon, 2022), the displacement of the VSD remains the main factor governing the speed and voltage dependence of the activation. Thus, changes in the extracellular Mg^{2+} concentration, which are known to interfere with the movement of the VSD

(Silverman et al., 2004; Bannister et al., 2005), cause a shift of the voltage dependence and activation speed that affects both gating components (**Fig. 3**), but not the transition between them.

The biphasic behavior arises from a different conductance between the two open states, larger for O_1, that results in a decrease in current amplitude as the channels leave O_1 and transition to O_2. Since the time required to access the two states is different, when short alternating stimuli are applied, each with a too short duration to allow entry into O_2, the different conductance results in a larger current amplitude than when a single sustained stimulus is used (**Fig. 4**). The presence of a second state with larger conductance when the integrity of the ring is compromised could explain the larger current amplitudes observed in heteromeric $K_V11.1$ (HERG1a/1b) channels, which lack at least one PAS domain as a result of alternative splicing and are crucial for proper cardiac repolarization (Feng et al., 2021). Thus, the second open state could also have physiological relevance in naturally occurring channel complexes.

Access to O_1 is favored from deep deactivated states, which appear important in other aspects of $K_V10.1$ channel function (e.g., Cole-Moore shift). Our conclusion is based on the changes in amplitude observed with different pre-pulse potentials (that is, driving the population to deep closed states, **Fig. 6A and B**) and on the behavior of a mutant known to hinder access to such deactivated states (L322H), which, when combined with mutations revealing O_1, shows limited access to this state (**Fig. 6C and D**).

Ca^{2+}-CaM is an important modulator of $K_V10.1$ that reduces WT current amplitude in the presence of elevated Ca^{2+} levels. A paradoxical current increase had been described for some of the mutants used in this study (Lörinczi et al., 2016), and we speculated that the presence of O_1 could be the basis for this phenomenon. Indeed, the elevation of intracellular Ca^{2+} leads to a transient loss of the biphasic behavior and larger current amplitude of the mutants compatible with a larger fraction of channels in O_1. Because access to O_1 occurs from deep closed states, this could be explained by an increased occupancy of such deactivated states in response to CaM binding. This appears to be the case since CaM induces a biphasic behavior in the mutant channels that show reduced access to deep closed states; thus, L322H mutants behave like the parental variants in the presence of Ca^{2+}-CaM. This implies a mechanistic explanation for the effect of Ca^{2+}-CaM on WT since favoring entry into deep closed states would result in a decrease in current amplitude in the absence of (a permeable) O_1.

Our initial hypothesis that CaM participates constitutively in the gating machinery of the channel, based on the loss of biphasic behavior when the C-terminal binding site for CaM was mutated (**Fig. 7D**), is unlikely to be correct because although there is a significant binding of CaM to the channel at basal intracellular Ca^{2+}, this fraction of channels, combined with the strong increase in bound CaM in the presence of high Ca^{2+} and the variable intracellular basal Ca^{2+} in oocytes would be insufficient to explain the qualitatively consistent behavior of the current of the different mutants. We speculate that the effects of the mutations in CaM binding sites are more related to their location in the protein than to their ability to bind CaM.

In summary, the gating of $K_V10.1$ (and similar channels) consists of a sequence of events that affect the voltage sensing domain, which moves in two sequential steps (Schonherr et al., 1999) and whose movement is transferred to the pore domain through intramolecular interactions (Bassetto et al., 2023). The voltage sensor maintains the gate closed (Mandala and MacKinnon, 2022), and its displacement has a permissive effect on gate opening. Once this restrictive factor is removed, a second step, most likely corresponding to a rotation of the intracellular ring, occurs and finally allows the gate to relax to the open state (Patlak, 1999). This final step is the only one directly observed in WT channels.

The presence of O_1 allowed us to model the behavior of the mutant channels based on a sequential "standard" Markovian model (**Fig. 8** and its supplements). To recapitulate the experimental data, our model proposes two levels of deactivated states, one corresponding structurally to the displacement of the VSD, and one to the conformation of the intracellular ring. O_1 would be accessible when the movement of the VSD is partially completed, and O_2 would require both events to occur. The model recapitulates the biphasic activation in the I-V and G-V curves. It also accounts also for the complex dependence of test-pulse voltage and time in tail currents. After weak depolarization, the tail-currents originate almost entirely from the mutant-specific open state O_1, while after strong depolarization, O_2-mediated currents dominate in the beginning, while at later times an increasingly populated O_1 overcomes the fast deactivation of channels in O_2. O_1 then deactivates with a much slower kinetics.

The model also predicts the behavior of mutant channels under short alternating stimuli between -20 and +50 mV. The current amplitude is larger under these conditions than during constant pulses to +50 mV. Furthermore, it also accounts for the increased current amplitude observed after hyperpolarizing conditioning pulses, that is, when accessing from deep closed states (**Suppl 3 to Fig.8**). The binding of Ca^{2+}-CaM is implemented in the model through change in the activation energy, corresponding to a shift in the equilibrium voltage of the gating transitions. The decomposition of the current into the individual open states' contribution shows that for increasing voltage shifts – representing high $[Ca^{2+}]_i$ – the mutant-specific O_1 closes later into the ramp, until eventually all current is carried by O_1.

Still, our model does not account for certain kinetic features of the channel, most evidently the continued increase in current amplitude when the model predicts that steady-state should be achieved (**Supp. 6 to Fig. 8**).

In summary, this study presents a more complete description of the gating mechanism of $K_V10.1$ channel, which can be extended to other members of the *KCNH* family. In response to depolarization, the movement of the voltage sensor would have a permissive role for the opening of the gate. The rotation of the intracellular ring would be the effective unlocking mechanism allowing permeation. This has profound implication pertaining the possibilities of fine tuning of gating, since the intracellular ring is more susceptible of posttranslational modifications and protein-protein interactions than the transmembrane domains. Our current knowledge of the physiology and pathophysiology of $K_V10.1$ indicate that the channel is relevant for the regulation of excitability acting at potentials close to the resting, rather than during active electrical signaling. Therefore, sustained modulation of gating, possible through modification of the intracellular ring, would be crucial for channel function. Since they allow dissection of the ring-dependent effect, our mutants will allow for a direct study of such modulation mechanisms,

Materials and Methods

Constructs

Mutants were generated using $K_V10.1$ (hEAG1) cloned in pSGEM (M. Hollmann, Bochum University) as a template (Jenke et al., 2003). The deletion mutants, Δ2-10 and ΔPASCap, were generated using In-Fusion HD Cloning kit (Clontech (TaKaRA)) following the supplier's instructions. For each construct we designed two primers, each of them with two regions: a 3' region that anneals to the template immediately up- or downstream of the sequence to be deleted, and a 5' that does not bind to the template but overlaps with the second primer (**Table S3**). The subsequent PCR amplification will then omit the sequence between the hybridization sites for the primers.

To generate the point mutations (ΔPASCap^{L322H}, ΔPASCap^{BDN}, ΔPASCap^{BDC2}, E600R^{L322H}, E600R^{BDN}, E600R^{BDC2}), site-directed mutagenesis was performed using Quick Change II XL kit (Agilent Technologies) using the primers listed in **Table S3**. E600R.pLeics71 and Δeag.pLeics71 were a gift from Dr. John Mitcheson, University of Leicester.

The expression construct for 5-myc-calmodulin was obtained by restriction cloning of CALM1 from pKK233-hCaM, which was a gift from Emanuel Strehler (Addgene plasmid # 47598) (Rhyner et al., 1992) into a pSGEM construct with five consecutive repeats of the myc tag (Lörinczi et al., 2015) using NcoI and HindIII (New England Biolabs).

All plasmids were linearized with NheI, and cRNA was synthesized using mMESSAGE mMACHINE T7 Transcription kit (Invitrogen Ambion).

Two-Electrode Voltage-Clamp Recordings

Oocyte preparation and injection were performed as described (Stuhmer, 1992). The amount of cRNA injected depended on the current amplitude obtained with each construct: 0.075 - 0.5ng/oocyte (WT and point mutation), 0.075-5ng/oocyte (deletion mutants), and 8-10ng/oocyte (split channels). Oocytes were maintained at 18 °C in ND96 buffer (in mM: 96 NaCl, 2 KCl, 1.8 $CaCl_2$, 1 $MgCl_2$, 5 HEPES, 2.5 Na-pyruvate, 0.5 Theophylline, pH 7.55). Tetracycline (USB) (50µg/ml), Amikacin (Enzo) (100µg/ml) and Ciprofloxacin (Enzo) (100µg/ml) were added as recommended in (O'Connell et al., 2011).

Two-electrode voltage-clamp (TEVC) recordings were performed 1-5 days after oocyte injection. The intracellular electrodes had a resistance of 0.4-1.5 MΩ when filled with 2M KCl. Normal Frog Ringer solution (NFR): (in mM: 115 NaCl, 2.5 KCl, 10 HEPES, 1.8 $CaCl_2$, pH 7.2), was used as external solution. Higher K^+ concentration (mM: 60 KCl, 57.5 NaCl, 10 HEPES, 1.8 $CaCl_2$, pH=7.4), was used instead to examine tail currents. Cl^- free NFR (in mM: 115 Na-methanesulfonate, 2.5 KOH, 10 HEPES, 1.8 $Ca(OH)_2$, pH=7.2), was used to limit current contamination with Cl^- current; in this case, agar bridges (2% agar in 3M NaCl) were used for the reference electrodes. To raise the intracellular Ca^{2+} concentration (Lörinczi et al., 2016), 5µM ionomycin (Abcam) and 5µM Thapsigargin (Abcam) were added to the bath. Ionomycin and Thapsigargin 5mM stocks was prepared using DMSO and diluted in the recording medium (Cl^- free NFR) immediately before recording. The final concentration of DMSO was thus 0.1%.

Data acquisition was performed using a TurboTEC 10-CD amplifier (npi Electronics) and the ITC-16 interface of an EPC9 patch-clamp amplifier (HEKA Elektronik). The current was filtered at 1.3 KHz and sampled at 10 KHz. Patchmaster software (HEKA Elektronik) was used to design and apply the stimulus protocols applied. Because of the profound effects of hyperpolarization on channel kinetics, leak subtraction was avoided except when explicitly indicated. Fitmaster (HEKA Elektronik) and IgorPro (WaveMetrics) were then used to analyze the recordings.

Most conductance-voltage plots are obtained for recordings with $[K^+]_{ext}$ =60mM. In this condition, tail currents are large and allow precise estimation of the reversal potential V_{eq}. Under this condition, the difference between intra- and extracellular potassium concentration is small and the Goldman-Hodgkin-Katz flux equation predicts a nearly linear relation. In these cases, conductance was calculated from the end-pulse current after measuring the reversal potential (V_{eq}) using:

$$G = I/(V_m - V_{eq}) \qquad \text{Eq.2}$$

where I is the current amplitude and V_m the stimulus. Conductance was then normalized to the maximum value and plotted against voltage stimulus. For WT recordings (**Fig. 1B**), a sigmoidal response was then fitted with a Boltzmann equation:

$$f(V) = \left(1 + \exp\left((V_h - V_m)/K\right)\right)^{-1} \quad \text{Eq.3}$$

With V_h being the voltage for half-maximal activation, K the slope factor and V_m the membrane potential as above.

The biphasic response we observed in the mutants was described with two sigmoidal components and a weight W to represent the transition between the two components. The equation used was as follows:

$$f(V) = A_o + \left(1 - \mathrm{W}(V)\right) \cdot \mathrm{A}_1 \cdot \left(1 + e^{(V_{h1} - V_m)/K_1}\right)^{-1} + \mathrm{W}(V) \cdot \mathrm{A}_2 \cdot \left(1 + e^{(V_{h2} - V_m)/K_2}\right)^{-1}$$

$$\mathrm{W}(V) = \left(1 + e^{(V_{h3} - V_m)/K_3}\right)^{-1} \quad \text{Eq.4}$$

If the currents were recorded in $[K^+]_{ext}$=2.5 mM, the driving force for currents becomes considerably non-linear (Kotler et al., 2022)and we estimated the conductance based on the full Goldman-Hodgkin-Katz flux equation for a current surface density Φ.

$\Phi = P \cdot P^{open} \cdot zF \cdot \frac{V_m}{V_T}\left(\frac{[K^+]_{in} - [K^+]_{out} \cdot e^{-V_m/V_T}}{1 - e^{-V_m/V_T}}\right)$, where $V_T = \frac{RT}{zF}$, with the gas constant *R*, the Faraday constant *F*, the absolute temperature *T*, the potassium channel open probability P^{open}, and the maximum permeability *P*. The ions valence *z* equals 1. Because we only work with normalized conductances, the following relation can be used to determine the voltage dependent conductance:

$$G(V) \propto I \cdot \left(\frac{1 - e^{-V_m/V_T}}{[K^+]_{in} - [K^+]_{out} e^{-V_m/V_T}}\right) \cdot \frac{V_T}{zFV_m}$$

Eq.5

Pull-down

Xenopus laevis oocytes were co-injected with RNA coding for 5xmyc-calmodulin (10ng) and K_V10.1 (0.5ng). Oocytes were lysed 72 h after injection through mechanical disruption in lysis buffer and incubation for 30 min on ice. The lysis buffer (1% Triton X-100, 150 mM NaCl, 50 mM HEPES pH 7.4, cOmplete EDTA-free protease inhibitor cocktail (Roche)) contained different free Ca^{2+} concentrations (0 nM, 20 nM, 50 nM, 100 nM, 500 nM, 1µM). To obtain accurate Ca^{2+} concentrations, EGTA was titrated with $CaCal_2$, to prepare 100mM CaEGTA stock solution as described in (Tsien and Pozzan, 1989). CaEGTA and EGTA were then added to the lysis buffer, adjusting EGTA/CaEGTA to control the concentration of free Ca^{2+} taking into account pH, ionic strength and temperature of solution using MaxChelator (Bers et al., 2010) As controls, non-injected oocytes, and oocytes injected with only K_V10.1 or 5xmyc-calmodulin were lysed in a Ca^{2+} free buffer.

The lysate was then centrifuged (20,000 x*g*) at 4 °C for 3 min to remove debris. 10% of the supernatant was set aside to load on the gel as input control. The lysate was pre-cleared using protein G magnetic beads (New England Biolabs). The cleared supernatant was then incubated with 3 µg anti-myc antibody (SIGMA M4439 monoclonal anti c-myc or Abcam ab206486 rat mAb to myc tag (9E10)) for 1.5h at 4 °C. Protein G magnetic beads were then added and incubated for 1.5h at 4 °C in rotation. After magnetic retrieval, the beads were washed three times using 0.1% Triton X-100, 300 mM NaCl, 50 mM HEPES pH 7.4, cOmplete (EDTA-free protease inhibitor cocktail), EGTA

and CaEGTA to obtain the corresponding Ca^{2+}-free concentrations (see above). Electrophoresis and immunoblotting conditions were as previously described (Lörinczi et al., 2015) using an anti-Myc (Sigma, 1:1000) or an anti-K_V10.1 antibody (Chen et al., 2011) overnight.

Acknowledgements

We thank the expert technical assistance of Kerstin Dümke. RA was supported by an IMPRS Neurosciences scholarship.

Data availability

The authors declare that the data supporting the findings of this study are available within the paper and its supplementary information files.

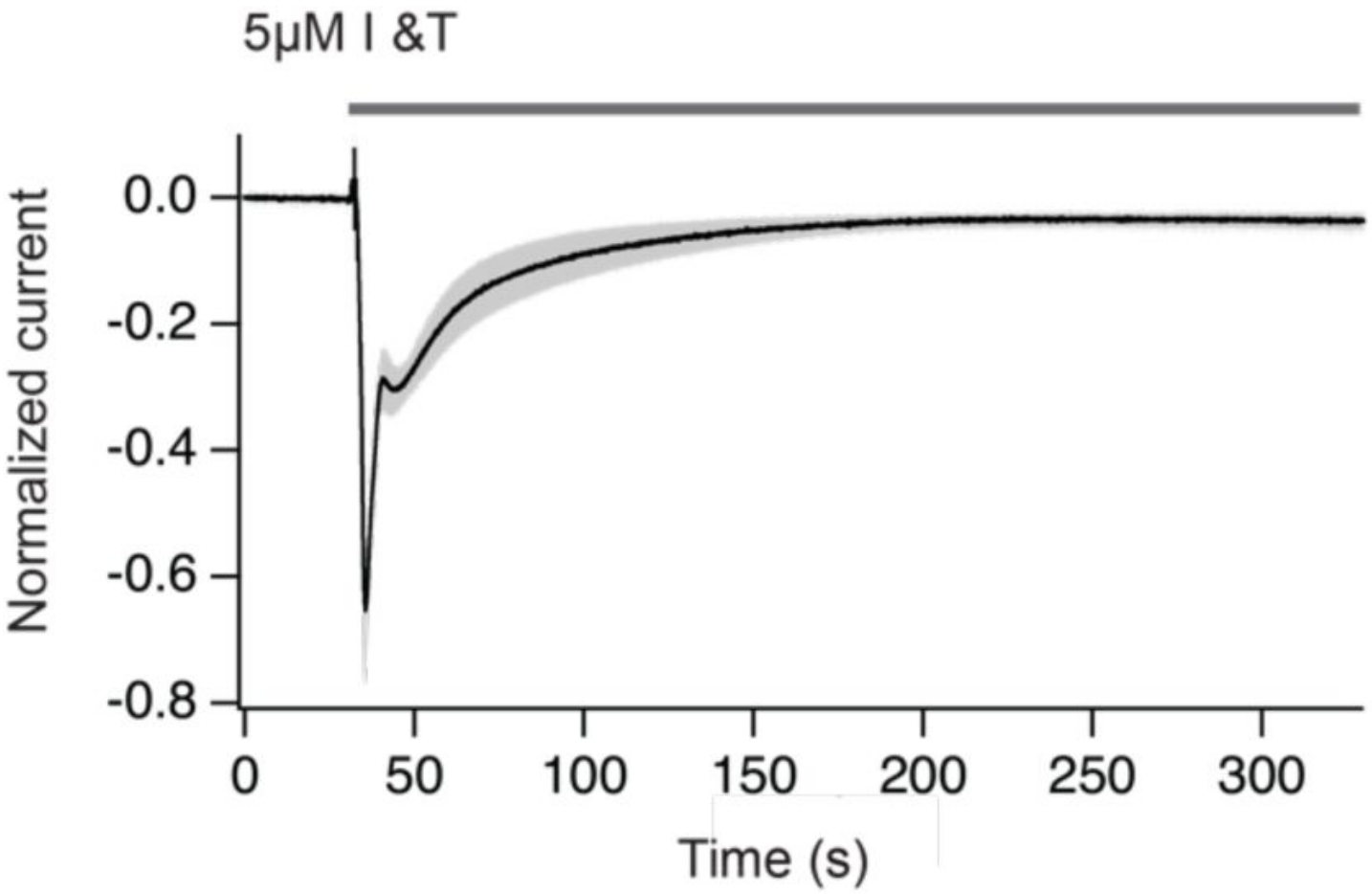

Supplement 1 to Figure 7.

Chloride currents obtained upon treatment with ionomycin plus thapsigargin. The increase in cytosolic Ca^{2+} translates in a Cl^- current that can be used to estimate the amplitude and duration of the Ca^{2+} increase. Notice that Ca^{2+} returns to basal levels in approximately 150 s. The gray area indicates SEM. N=9

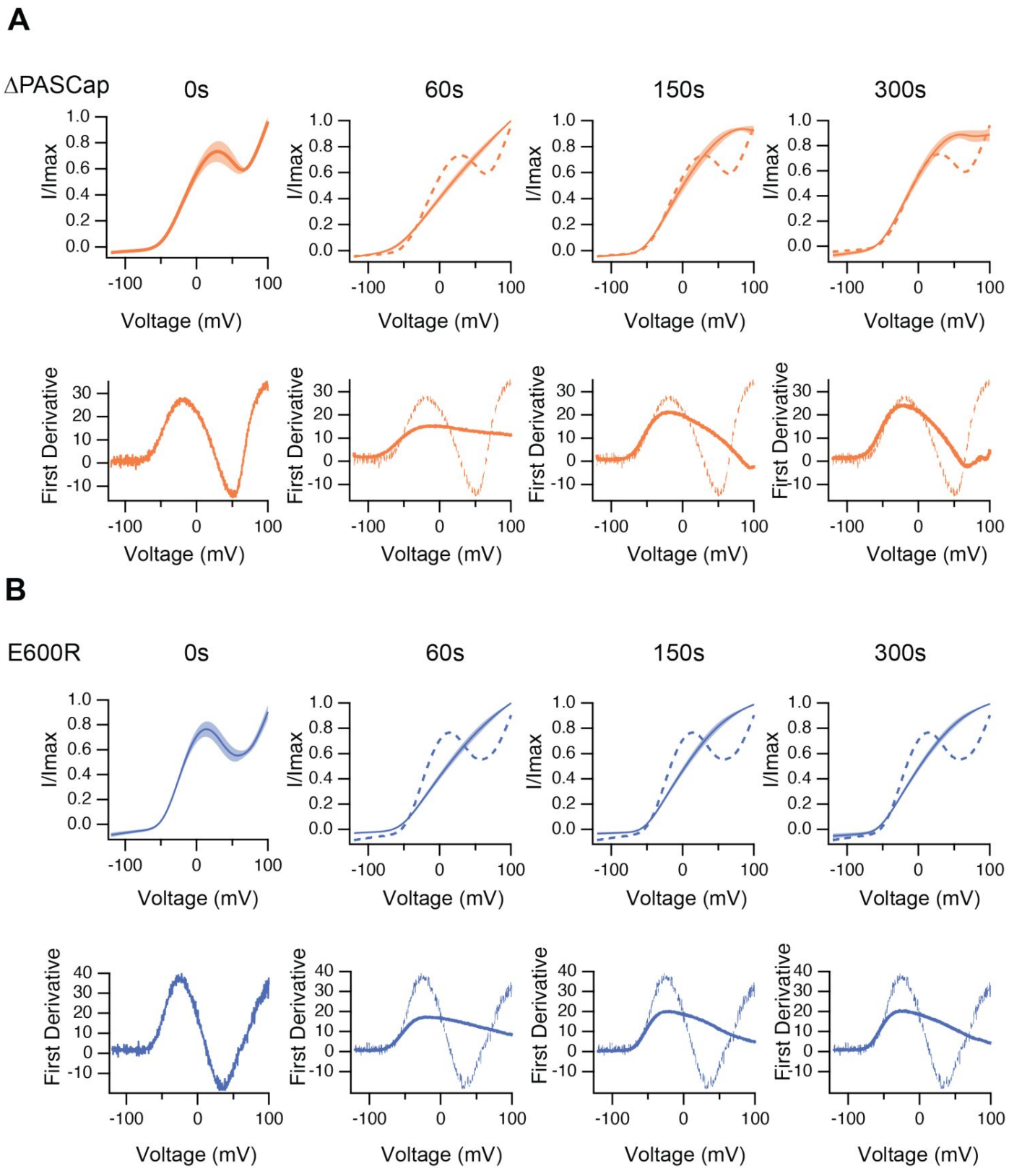

Supplement 2 to Figure 7.

The upper traces show the average of normalized ramps at the indicated times for ΔPASCap (**A**) and E600R (**B**) after induction of Ca^{2+} rise. At 60, 150 and 300 s, the dashed line corresponds to the ramp at time 0. The shadowed area indicates SEM (N: ΔPASCap = 8, E600R = 10). The lower panels correspond to the first derivative of the current traces to illustrate the changes in slope.

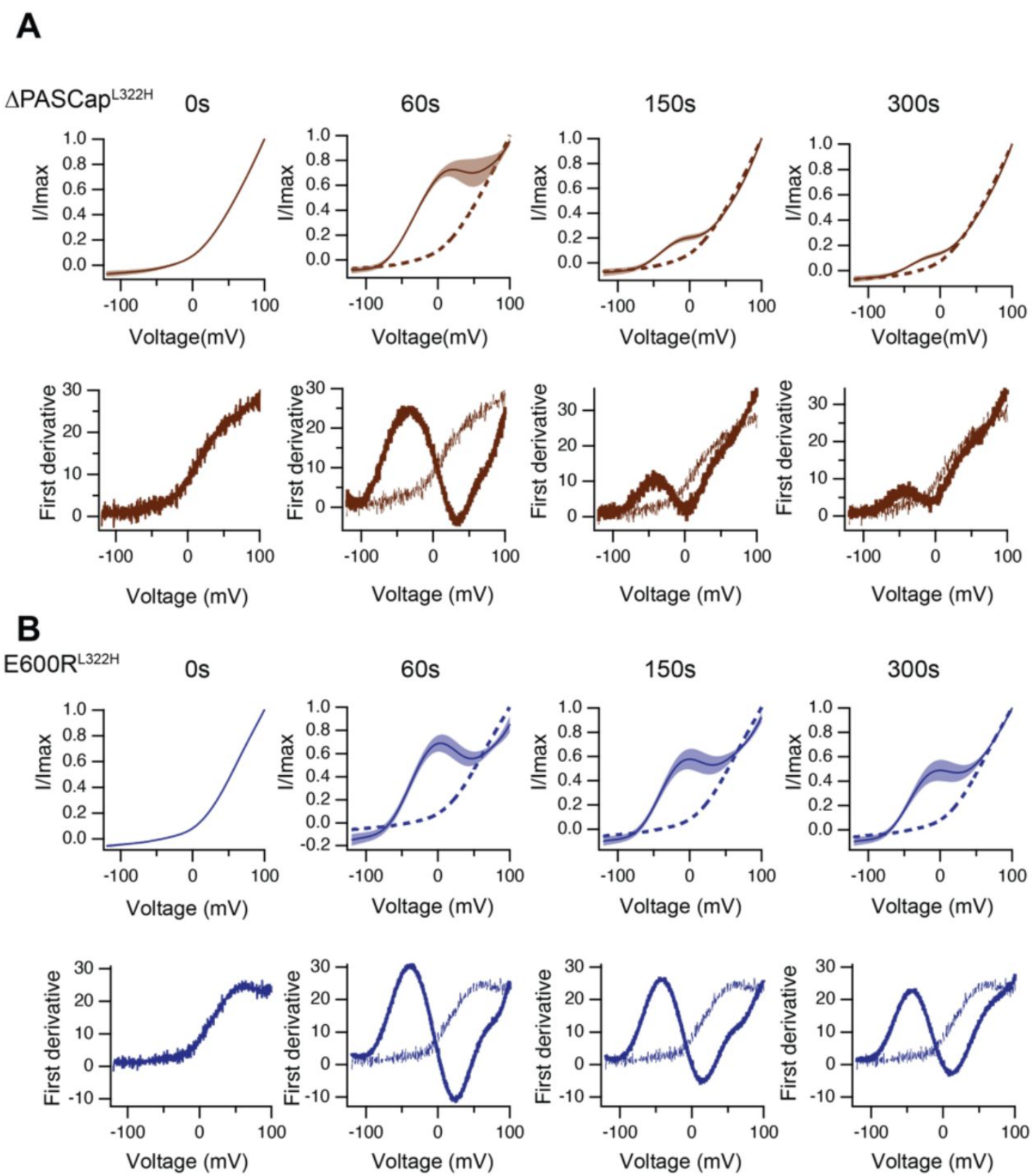

Supplement 3 to Figure 7.

Like in Supplement 2, the upper traces show the average of normalized ramps for ΔPASCap^{L322H} (**A**) and E600^{L322H} (**B**) at the indicated times after induction of Ca^{2+} rise. At 60, 150 and 300 s, the dashed line corresponds to the ramp at time 0. The shadowed area indicates SEM (N: ΔPASCap^{L322H} = 5, E600R^{L322H} = 11). The lower panels correspond to the first derivative of the current traces to illustrate the changes in slope.

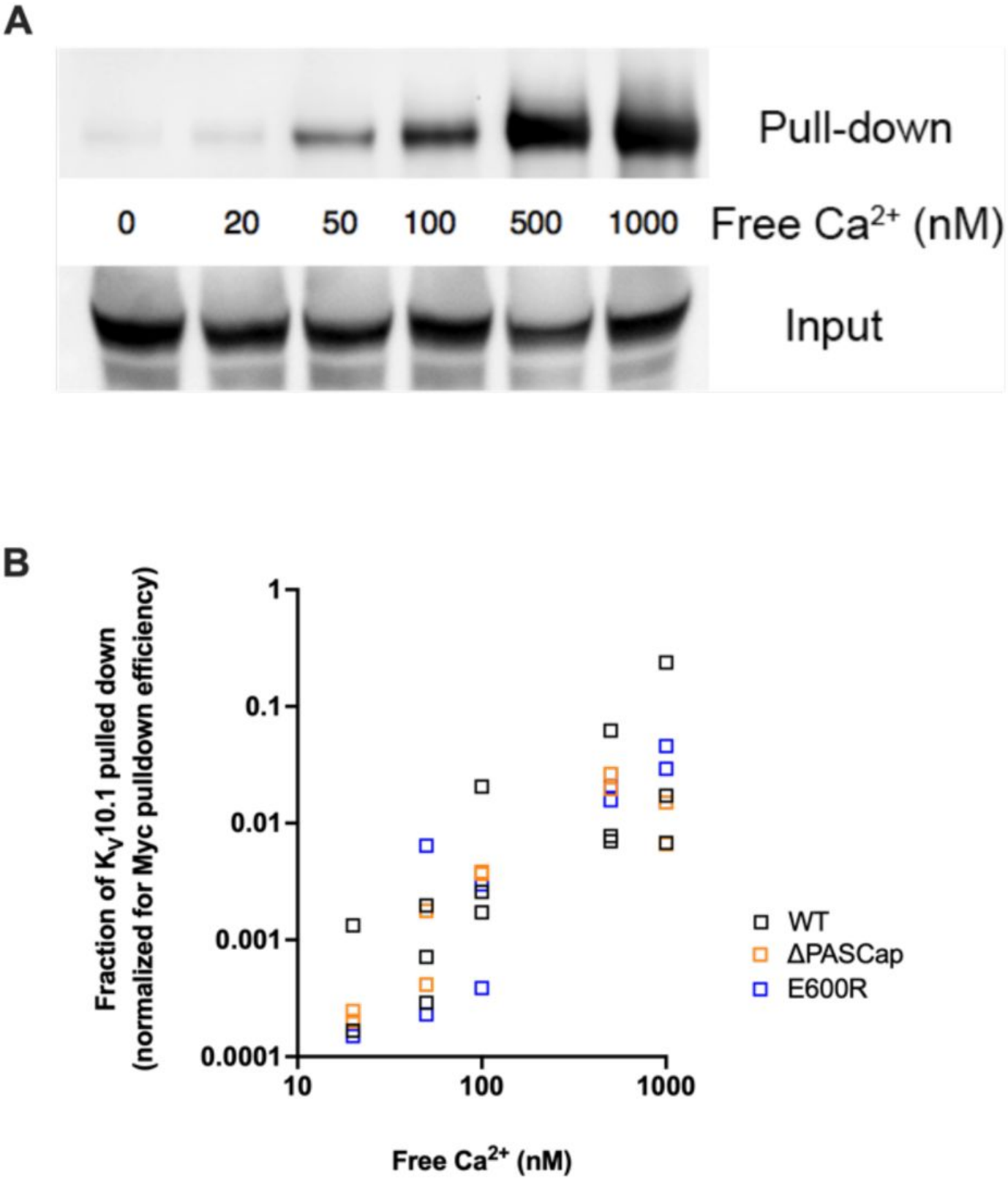

Supplement 4 to Figure 7.

A. Ca^{2+}-dependent binding of CaM to $K_V10.1$. CaM was precipitated with anti-Myc antibody and the resulting pulled down fraction was immunoblotted using polyclonal anti-$K_V10.1$ antibody. **B** Quantification of all experiments reveals a strong dependence on Ca^{2+} concentration in WT and to a similar extent in mutant channels. The fraction of $K_V10.1$ pulled down increases by two orders of magnitude in high Ca^{2+}.

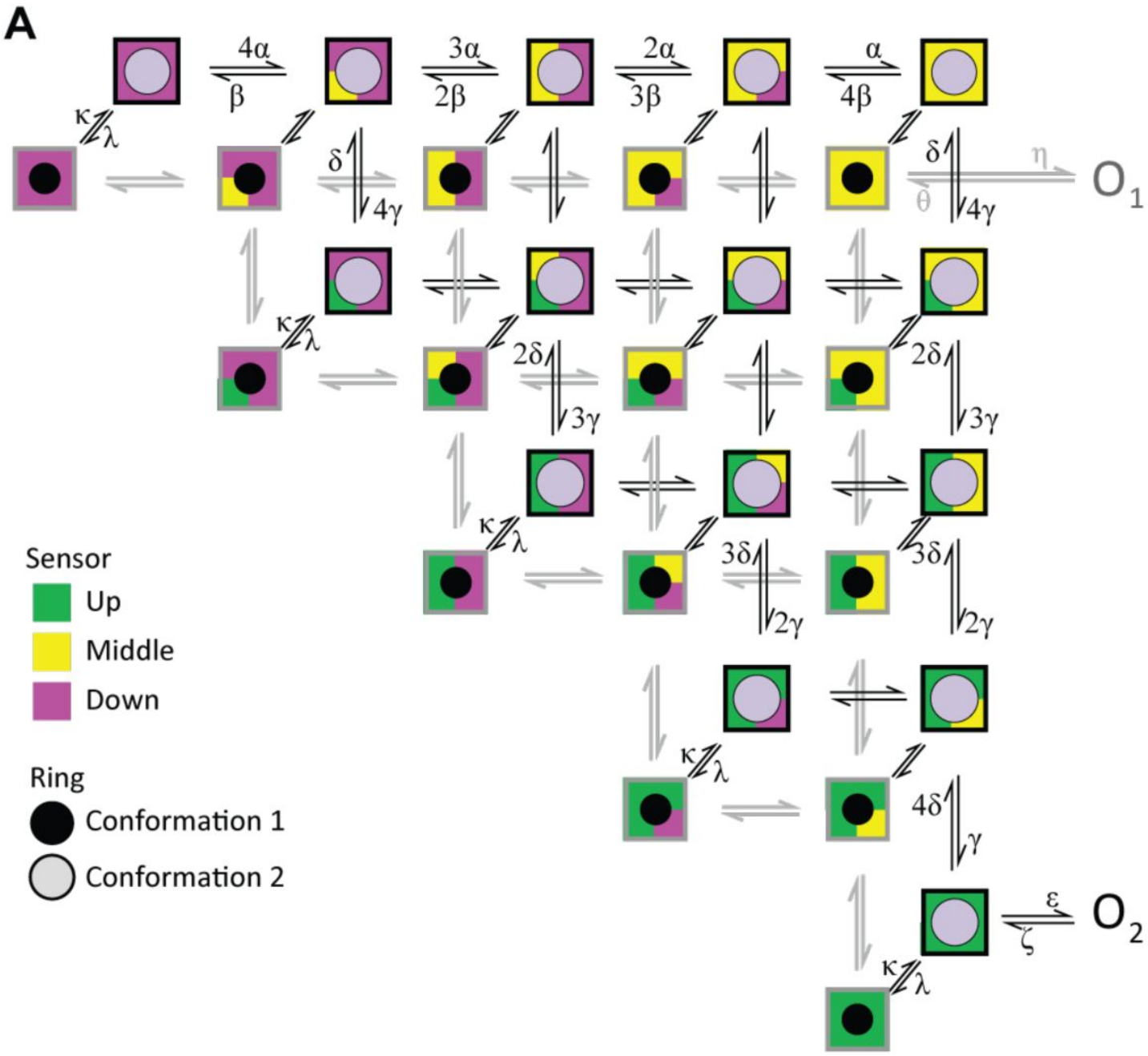

Supplement 1 to Figure 8.

Cartoon depicting the state model proposed.

A two-layer Markov-Model depicting possible conformations for the sensor and the ring. The sensor in each subunit can independently adopt one of three conformations (up, middle, and down) (Han et al., 2023). The up conformation represents the active conformation. The conformation of the ring changes across the two layers. The second conformation in the upper layer allows the channel to access "O_2" provided that all sensors are in the up conformation. Transitions within each layer is governed by (α, β, γ, δ), we proposed that the transitions are identical in the two layers. Transitions between the two levels are governed by the rate constants κ and λ

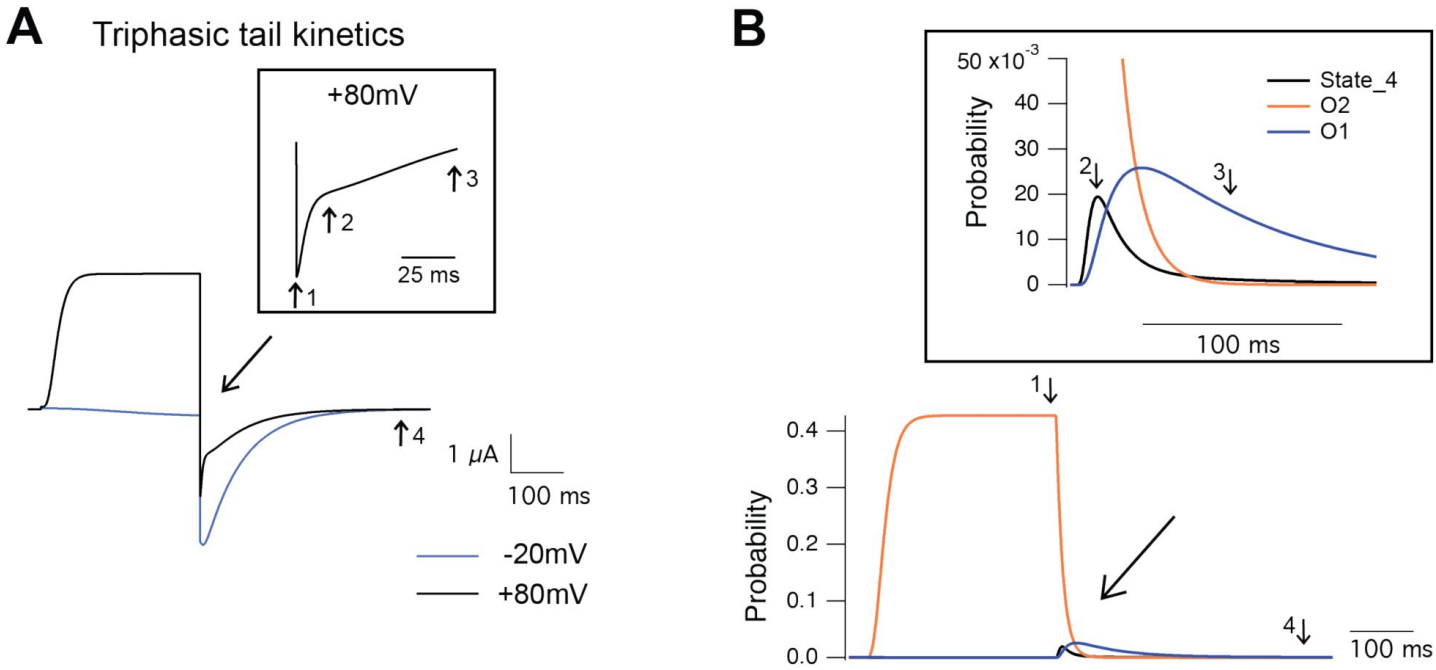

Supplement 2 to Figure 8.

Current simulations for ΔPASCap upon depolarization to -20 or +80 mV in the presence of high extracellular K^+. **A**. The triphasic current kinetics (see **Fig. 1E**) observed experimentally at +80 mV (insert) is predicted by the model. **B**. Occupancy of State_4 (state closest to O_1), O_1 and O_2 as a function of time during a depolarization to +80 mV.

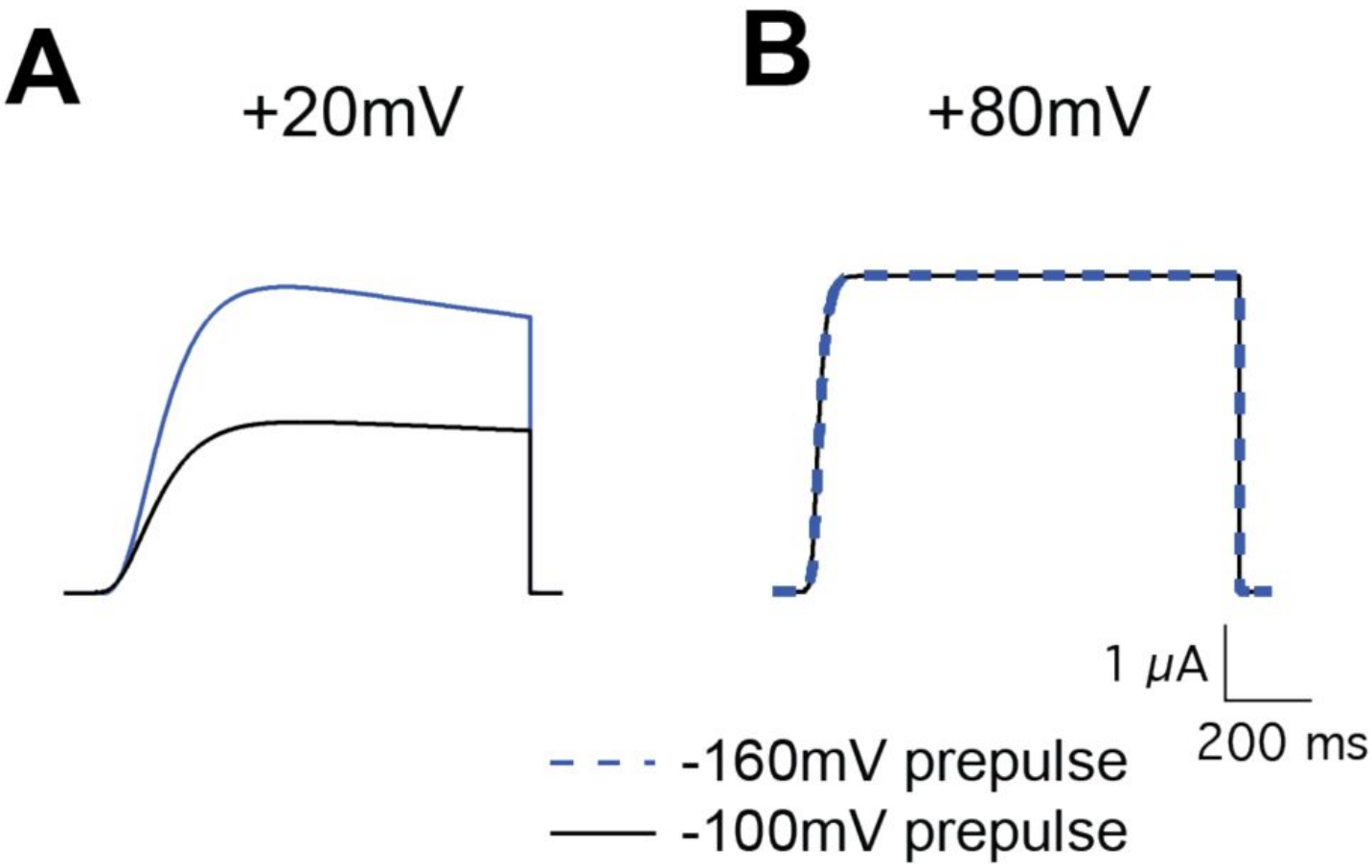

Supplement 3 to Figure 8.

Current simulations for ΔPASCap upon depolarization to +20 and +80 mV after a conditioning pulse to -160 or -120 mV. The current at +20 mV is larger after -160 mV, while the current at +80 mV is unaffected by the conditioning pulse (see **Fig. 6A**)

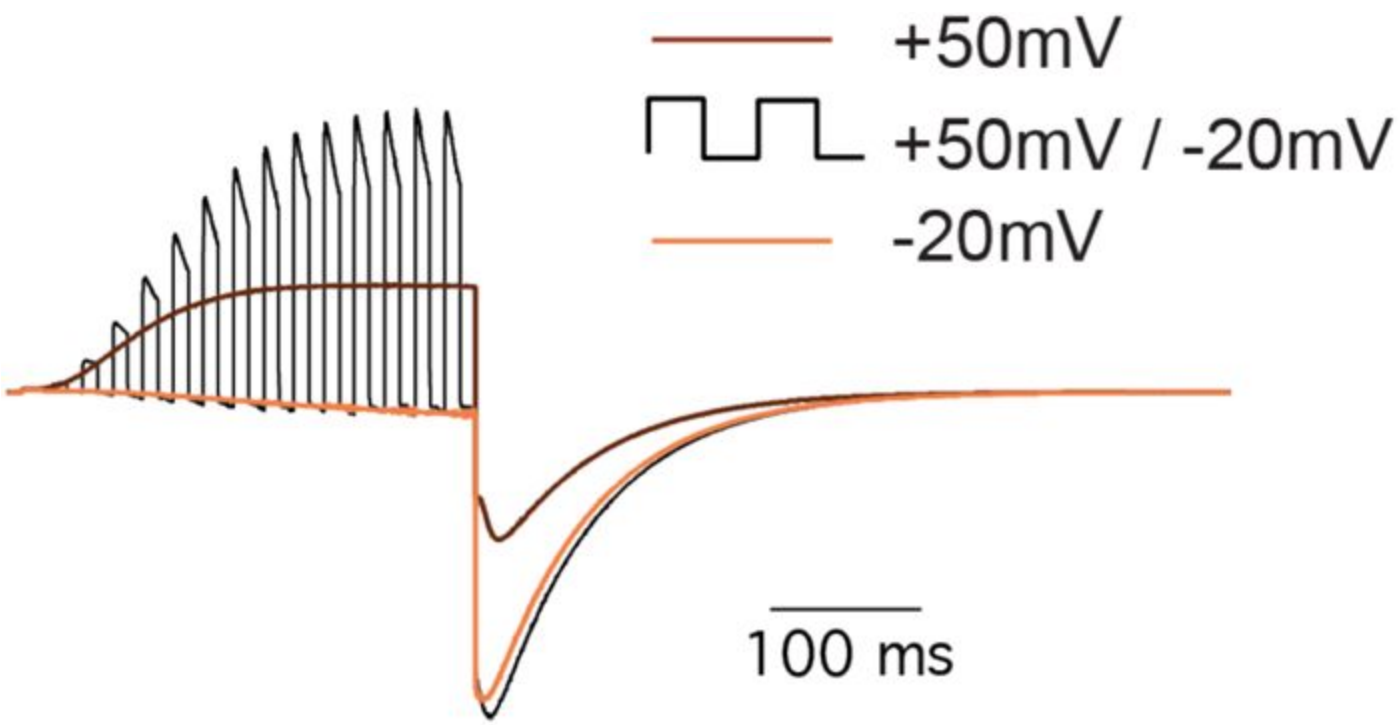

Supplement 4 to Figure 8.

Current simulations for ΔPASCap upon alternating stimuli between -20 and +50 mV, as compared to sustained depolarization to each of the potentials (see **Fig. 4B**)

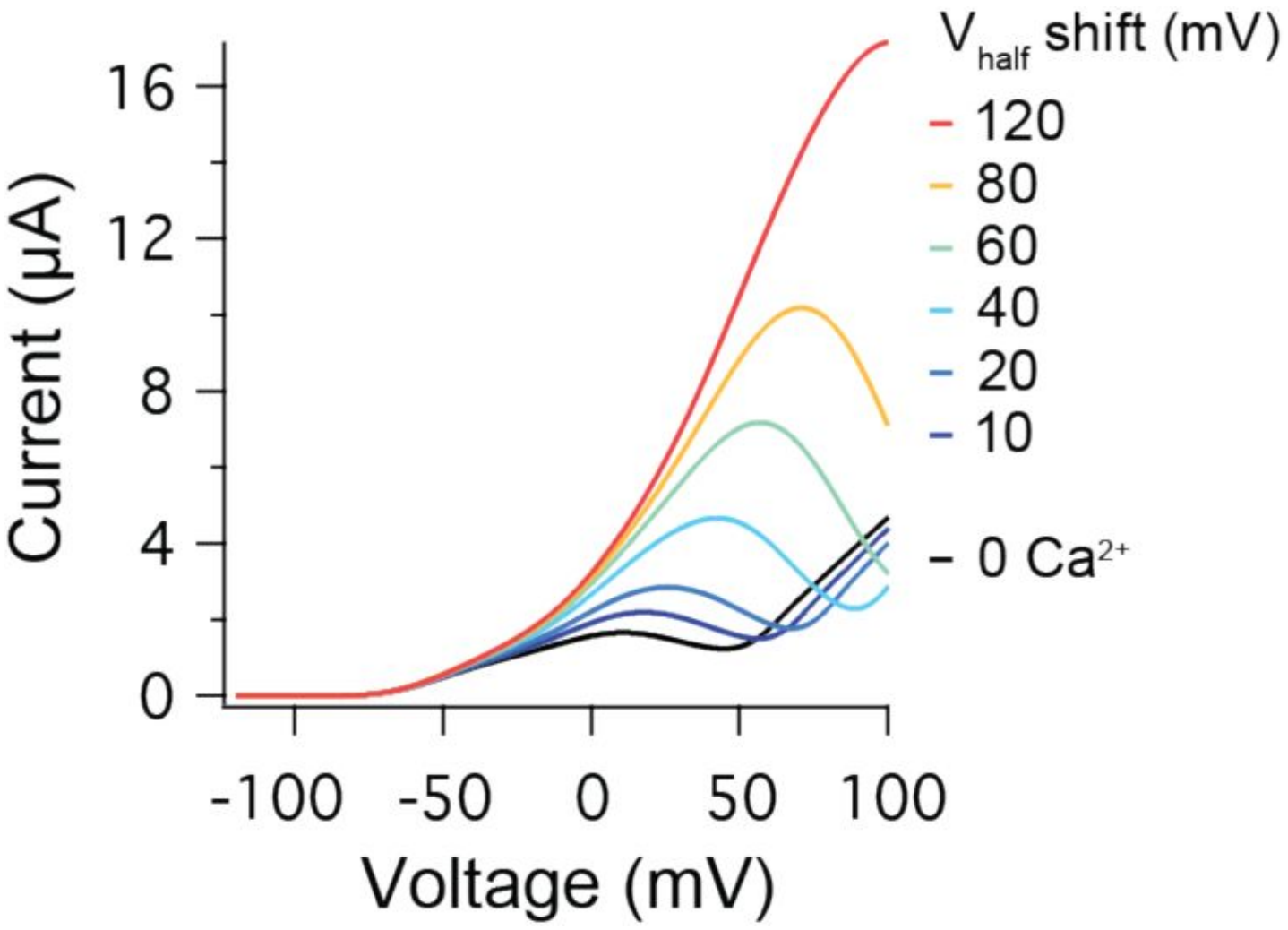

Supplement 5 to Figure 8.

Current simulations for ΔPASCap under ramp depolarization using shifted rate constants (γ, δ, κ) to mimic the effect of CaM binding (see **Fig. 7A**)

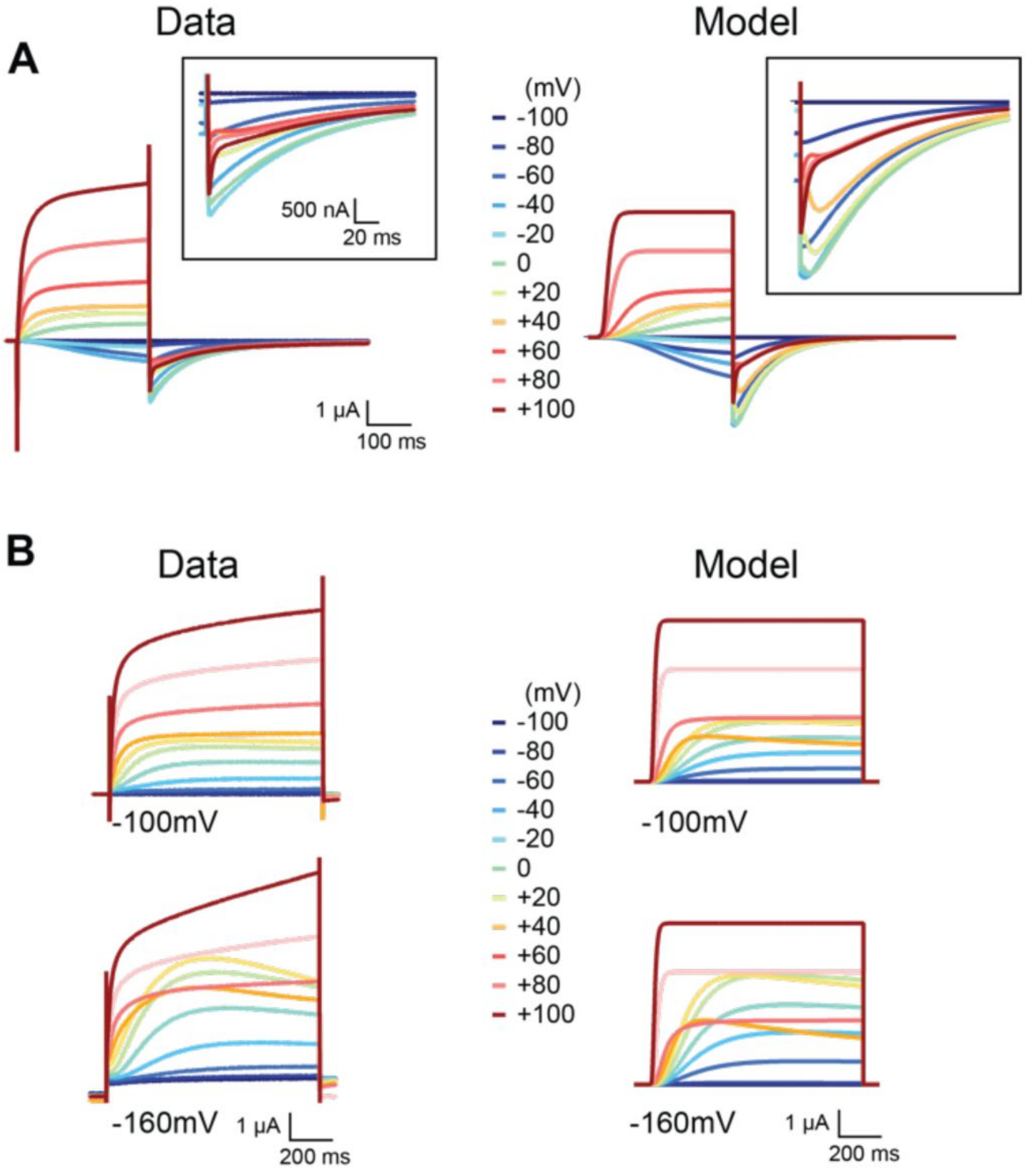

Supplement 6 to Figure 8.

Side-by-side comparison of experimental data and model prediction during depolarizations between -100 and +100 mV in the presence of high (**A**) or low extracellular K^+ (**B**). the model describes the features of the current except the sustained rising phase during strong depolarizations.

	Δ2-10	**Δ**PASCap	Δeag	E600R
A_0	-0.052	-0.054	-0.067	-0.091
A_1	1.78	1.78	1.32	2.99
Vh_1	-33.57	-33.57	-33.57	-33.57
K_1	16.38	16.38	16.38	16.38
A_2	1.31	1.18	0.25	0.99
Vh_2	51.63	79.63	102.70	83.04
K_2	46.05	25.38	6.41	22.51
Vh_3	-33.47	-5.16	55.52	-21.93
K_3	23.47	27.12	27.01	34.9

Table S1.

Parameters of a global fit that linked the first component of the biphasic response

rate x	x_0	A_x [s^{-1}]	V_{hx} [V]	K_x [V^{-1}]
α	8	192	0.09	-55
β	4	596	-0.13	80
γ	5	595	0.05	-30
δ	15	235	0.055	30
ε	200	0	—	—
ζ	120	0	—	—
η	100	400	0	-80
θ	20	80	0	-50
κ_R	0.125	69.875	-0.1	200
κ_L	0.125	499.875	0.09	-130
λ	0.1	999.9	-0.12	170

Table S2

parameters describing the voltage dependence of the transitions between states in the Markov model of K_V10.1 PASCap, in conjunction with Eq. 1.

Deletion/Mutation	Template (s)	Primers
2-10	pSGEM.Kv10.1 pSGEM Kv10.1 L341Split	F attcgatatcaagcttatggtggcccctcaaaacacgtttct R cggtatcgataagcttcagctggctccaaaaatgtctctct
ΔPASCap 2-25	pSGEM Kv10.1	F gctgccgccaccatg aatgatactaattttgtgttggggaa R catggtggcggcagctcg
ΔCNBHD 525-697	psGEM Kv10.1.	F tccagaggcattgac aatgaggccccctgatcttgc R gtcaatgcctctggacatggaccaa
L322H	pSGEM Kv10.1 ΔPASCap pSGEM Kv10.1 E600R	F gatgagggcatcagcagccatttcagctctctaaaagttgt R acaacttttagagagctgaaatggctgctgatgccctcatc
N-terminal CaM binding site (BDN) F151NL154N	pSGEM Kv10.1 Δ2-10 pSGEM Kv10.1 ΔPASCap	F151N ctcttgtcagccgagcattcttcccccagcctttac L154N tgcttgtcagtgctcttgtattccgagcattcttcccccag
C-terminal CaM binding site (BDC2) F714SF717S	pSGEM Kv10.1 Δ2-10 pSGEM Kv10.1 ΔPASCap	F714S gtcggaatctctggctgaggcgccggacag F717S ctgctgtcggcttctctggctgaggcgccgg

Table S3.

Primers used for infusion cloning or site-directed mutagenesis.

The sequences are listed 5'-3'. For mutagenesis primers, only the sense sequences are given. The reverse primers corresponded to the reverse-complement sequence.

References

1. Babu Y.S., Sack J.S., Greenhough T.J., Bugg C.E., Means A.R., Cook W.J (1985) **Three-dimensional structure of calmodulin** *Nature* **315**:37–40 https://doi.org/10.1038/315037a0

2. Bannister J.P., Chanda B., Bezanilla F., Papazian D.M (2005) **Optical detection of rate-determining ion-modulated conformational changes of the ether-a-go-go K+ channel voltage sensor** *Proc Natl Acad Sci U S A* **102**:18718–18723

3. Barros F., De La Pena P., Dominguez P., Sierra L.M., Pardo L.A. (2020) **The EAG Voltage-Dependent K(+) Channel Subfamily: Similarities and Differences in Structural Organization and Gating** *Front Pharmacol* **11** https://doi.org/10.3389/fphar.2020.00411

4. Bassetto C.a.Z., Costa F., Guardiani C., Bezanilla F., Giacomello A. (2023) **Noncanonical electromechanical coupling paths in cardiac hERG potassium channel** *Nat Commun* **14** https://doi.org/10.1038/s41467-023-36730-7

5. Bauer C.K., Schwarz J.R (2018) **Ether-à-go-go K+ channels: effective modulators of neuronal excitability** *The Journal of Physiology* **596**:769–783 https://doi.org/10.1113/JP275477

6. Bers D.M., Patton C.W., Nuccitelli R (2010) **A Practical Guide to the Preparation of Ca2+ a Buffers** *Calcium in Living Cells* **99**:1–26 https://doi.org/10.1016/S0091-679x(10)99001-8

7. Busa W.B., Nuccitelli R (1985) **An elevated free cytosolic Ca2+ wave follows fertilization in eggs of the frog, Xenopus laevis** *J Cell Biol* **100**:1325–1329 https://doi.org/10.1083/jcb.100.4.1325

8. Chen Y., Sánchez A., Rubio M.E., Kohl T., Pardo L.A., Stühmer W (2011) **Functional Kv10.1 Channels Localize to the Inner Nuclear Membrane** *PLoS ONE* **6** https://doi.org/10.1371/journal.pone.0019257

9. Codding S.J., Johnson A.A., Trudeau M.C (2020) **Gating and regulation of KCNH (ERG, EAG, and ELK) channels by intracellular domains** *Channels (Austin)* **14**:294–309 https://doi.org/10.1080/19336950.2020.1816107

10. Codding S.J., Trudeau M.C (2019) **The hERG potassium channel intrinsic ligand regulates N- and C-terminal interactions and channel closure** *J Gen Physiol* **151**:478–488 https://doi.org/10.1085/jgp.201812129

11. Cole K.S., Moore J.W (1960) **Potassium ion current in the squid giant axon: dynamic characteristic** *Biophys J* **1**:1–4

12. Dai G., James Z.M., Zagotta W.N (2018) **Dynamic rearrangement of the intrinsic ligand regulates KCNH potassium channels** *The Journal of General Physiology*

13. Dai G., Zagotta W.N (2017) **Molecular mechanism of voltage-dependent potentiation of KCNH potassium channels** *eLife* **6** https://doi.org/10.7554/eLife.26355

14. De La Pena P., Dominguez P., Barros F. (2018) **Gating mechanism of Kv11.1 (hERG) K(+) channels without covalent connection between voltage sensor and pore domains** *Pflugers Arch* **470**:517–536 https://doi.org/10.1007/s00424-017-2093-9

15. Feng L., Zhang J., Lee C., Kim G., Liu F., Petersen A.J., Lim E., Anderson C.L., Orland K.M., Robertson G.A., Eckhardt L.L., January C.T., Kamp T.J (2021) **Long QT Syndrome KCNH2 Variant Induces hERG1a/1b Subunit Imbalance in Patient-Specific Induced Pluripotent Stem Cell-Derived Cardiomyocytes** *Circ Arrhythm Electrophysiol* **14** https://doi.org/10.1161/CIRCEP.120.009343

16. Gianulis E.C., Liu Q., Trudeau M.C (2013) **Direct interaction of eag domains and cyclic nucleotide– binding homology domains regulate deactivation gating in hERG channels** *The Journal of General Physiology* **142**:351–366 https://doi.org/10.1085/jgp.201310995

17. Gonçalves J.T., Stühmer W (2010) **Calmodulin Interaction with hEAG1 Visualized by FRET Microscopy** *PLoS ONE* **5** https://doi.org/10.1371/journal.pone.0010873

18. Haitin Y., Carlson A.E., Zagotta W.N (2013) **The structural mechanism of KCNH-channel regulation by the eag domain** *Nature* **501**:444–448 https://doi.org/10.1038/nature12487

19. (1970) **http://www.nature.com/nature/journal/v501/n7467/abs/nature12487.html#supplementary-information**

20. Han S., Vance J., Jones S., Decata J., Tran K., Cummings J., Wang S (2023) **Voltage sensor dynamics of a bacterial voltage-gated sodium channel NavAb reveal three conformational states** *J Biol Chem* **299** https://doi.org/10.1016/j.jbc.2023.102967

21. Harley C.A., Bernardo-Seisdedos G., Stevens-Sostre W.A., Jones D.K., Azevedo M.M., Sampaio P., Lorga-Gomes M., Trudeau M.C., Millet O., Robertson G.A., Morais-Cabral J.H (2021) **Conformation-sensitive antibody reveals an altered cytosolic PAS/CNBh assembly during hERG channel gating** *Proc Natl Acad Sci U S A* **118** https://doi.org/10.1073/pnas.2108796118

22. Hoshi T., Armstrong C.M (2015) **The Cole-Moore Effect: Still Unexplained?** *Biophys J* **109**:1312–1316 https://doi.org/10.1016/j.bpj.2015.07.052

23. James Z.M., Zagotta W.N (2017) **Structural insights into the mechanisms of CNBD channel function** *The Journal of General Physiology* https://doi.org/10.1085/jgp.201711898

24. Jenke M., Sanchez A., Monje F., Stuhmer W., Weseloh R.M., Pardo L.A (2003) **C-terminal domains implicated in the functional surface expression of potassium channels** *EMBO J* **22**:395–403 https://doi.org/10.1093/emboj/cdg035

25. Ju M., Wray D (2006) **Molecular regions responsible for differences in activation between heag channels** *Biochem Biophys Res Commun* **342**:1088–1097

26. Kotler O., Gutnick M.J., Fleidervish I.A (2022) **In computational models, action potential propagation in ultrathin axons is resilient despite considerable intracellular Na(+) accumulation** *Proc Natl Acad Sci U S A* **119** https://doi.org/10.1073/pnas.2120782119

27. Lörinczi É., Gómez-Posada J.C., De La Peña P., Tomczak A.P., Fernández-Trillo J., Leipscher U., Stühmer W., Barros F., Pardo L.A. (2015) **Voltage-dependent gating of KCNH potassium channels lacking a covalent link between voltage-sensing and pore domains** *Nat Commun* **6** https://doi.org/10.1038/ncomms7672

28. Lörinczi E., Helliwell M., Finch A., Stansfeld P.J., Davies N.W., Mahaut-Smith M., Muskett F.W., Mitcheson J.S (2016) **Calmodulin Regulates Human Ether à Go-Go 1 (hEAG1) Potassium Channels through Interactions of the Eag Domain with the Cyclic Nucleotide Binding Homology Domain** *Journal of Biological Chemistry* **291**:17907–17918 https://doi.org/10.1074/jbc.M116.733576

29. Ludwig J., Terlau H., Wunder F., Bruggemann A., Pardo L.A., Marquardt A., Stuhmer W., Pongs O (1994) **Functional expression of a rat homologue of the voltage gated either a go-go potassium channel reveals differences in selectivity and activation kinetics between the Drosophila channel and its mammalian counterpart** *EMBO J* **13**:4451–4458

30. Malak O.A., Gluhov G.S., Grizel A.V., Kudryashova K.S., Sokolova O.S., Loussouarn G (2019) **Voltage-dependent activation in EAG channels follows a ligand-receptor rather than a mechanical-lever mechanism** *J Biol Chem* https://doi.org/10.1074/jbc.RA119.007626

31. Mandala V.S., Mackinnon R (2022) **Voltage-sensor movements in the Eag Kv channel under an applied electric field** *Proc Natl Acad Sci U S A* **119** https://doi.org/10.1073/pnas.2214151119

32. Nunez E., Muguruza-Montero A., Villarroel A (2020) **Atomistic Insights of Calmodulin Gating of Complete Ion Channels** *Int J Mol Sci* **21** https://doi.org/10.3390/ijms21041285

33. O'connell D., Mruk K., Rocheleau J.M., Kobertz W.R (2011) **Xenopus laevis oocytes infected with multi-drug–resistant bacteria: implications for electrical recordings** *The Journal of General Physiology* **138**:271–277 https://doi.org/10.1085/jgp.201110661

34. Parker I., Choi J., Yao Y (1996) **Elementary events of InsP3-induced Ca2+ liberation in Xenopus oocytes: hot spots, puffs and blips** *Cell Calcium* **20**:105–121 https://doi.org/10.1016/s0143-4160(96)90100-1

35. Patlak J.B (1999) **Cooperating to unlock the voltage-dependent K channel** *J Gen Physiol* **113**:385–388 https://doi.org/10.1085/jgp.113.3.385

36. Rhyner J.A., Koller M., Durussel-Gerber I., Cox J.A., Strehler E.E (1992) **Characterization of the human calmodulin-like protein expressed in Escherichia coli** *Biochemistry* **31**:12826–12832 https://doi.org/10.1021/bi00166a017

37. Sahoo N., Schonherr R., Hoshi T., Heinemann S.H (2012) **Cysteines control the N- and C-linker-dependent gating of KCNH1 potassium channels** *Biochim Biophys Acta* **1818**:1187–1195 https://doi.org/10.1016/j.bbamem.2012.01.021

38. Schonherr R., Hehl S., Terlau H., Baumann A., Heinemann S.H (1999) **Individual subunits contribute independently to slow gating of bovine EAG potassium channels** *Journal of Biological Chemistry* **274**:5362–5369

39. Schonherr R., Lober K., Heinemann S.H (2000) **Inhibition of human ether a go-go potassium channels by Ca(2+)/calmodulin** *Embo J* **19**:3263–3271

40. Silverman W.R., Bannister J.P.A., Papazian D.M (2004) **Binding Site in Eag Voltage Sensor Accommodates a Variety of Ions and is Accessible in Closed Channel** *Biophysical Journal* **87**:3110–3121 https://doi.org/10.1529/biophysj.104.044602

41. Silverman W.R., Tang C.Y., Mock A.F., Huh K.B., Papazian D.M (2000) **Mg(2+) modulates voltage-dependent activation in ether-a-go-go potassium channels by binding between transmembrane segments S2 and S3** *Journal of General Physiology* **116**:663–678 https://doi.org/10.1085/jgp.116.5.663

42. Stuhmer W (1992) **Electrophysiological recording from Xenopus oocytes** *Methods Enzymol* **207**:319–339

43. Tang C.-Y., Bezanilla F., Papazian D.M (2000) **Extracellular Mg2+ Modulates Slow Gating Transitions and the Opening of Drosophila Ether-à-Go-Go Potassium Channels** *The Journal of General Physiology* **115**:319–338 https://doi.org/10.1085/jgp.115.3.319

44. Terlau H., Heinemann S.H., Stuhmer W., Pongs O., Ludwig J (1997) **Amino terminal-dependent gating of the potassium channel rat eag is compensated by a mutation in the S4 segment** *Journal of Physiology* **502**:537–543 https://doi.org/10.1111/j.1469-7793.1997.537bj.x

45. Terlau H., Ludwig J., Steffan R., Pongs O., Stühmer W., Heinemann S (1996) **Extracellular Mg2+ regulates activation of rat eag potassium channel** *Pflügers Archiv European Journal of Physiology* **432**:301–312 https://doi.org/10.1007/s004240050137

46. Thouta S., Sokolov S., Abe Y., Clark Sheldon j, Cheng Yen m, Claydon Tom w (2014) **Proline Scan of the hERG Channel S6 Helix Reveals the Location of the Intracellular Pore Gate** *Biophysical Journal* **106**:1057–1069 https://doi.org/10.1016/j.bpj.2014.01.035

47. Tian M.Q., Li R.K., Yang F., Shu X.M., Li J., Chen J., Peng L.Y., Yu X.H., Yang C.J (2023) **Phenotypic expansion of KCNH1-associated disorders to include isolated epilepsy and its associations with genotypes and molecular sub-regional locations** *CNS Neurosci Ther* **29**:270–281 https://doi.org/10.1111/cns.14001

48. Tomczak A.P., Fernández-Trillo J., Bharill S., Papp F., Panyi G., Stühmer W., Isacoff E.Y., Pardo L.A (2017) **A new mechanism of voltage-dependent gating exposed by KV10.1 channels interrupted between voltage sensor and pore** *J Gen Physiol* **149**:577–593 https://doi.org/10.1085/jgp.201611742

49. Toplak Z., Hendrickx L.A., Abdelaziz R., Shi X., Peigneur S., Tomasic T., Tytgat J., Peterlin-Masic L., Pardo L.A (2022) **Overcoming challenges of HERG potassium channel liability through rational design: Eag1 inhibitors for cancer treatment** *Med Res Rev* **42**:183–226 https://doi.org/10.1002/med.21808

50. Tsien R., Pozzan T. (1989) **[14] Measurement of cytosolic free Ca2+ with quin2** *Methods in Enzymology* :230–262

51. Verkest C., Schaefer I., Nees T.A., Wang N., Jegelka J.M., Taberner F.J., Lechner S.G (2022) **Intrinsically disordered intracellular domains control key features of the mechanically-gated ion channel PIEZO2** *Nat Commun* **13** https://doi.org/10.1038/s41467-022-28974-6

52. Wang W., Mackinnon R (2017) **Cryo-EM Structure of the Open Human Ether-à-go-go - Related K+ Channel hERG** *Cell* **169**:422–430 https://doi.org/10.1016/j.cell.2017.03.048

53. Wang Z.-J., Soohoo S.M., Tiwari P.B., Piszczek G., Brelidze T.I (2020) **Chlorpromazine binding to the PAS domains uncovers the effect of ligand modulation on EAG channel activity** *Journal of Biological Chemistry, jbc.RA* **119** https://doi.org/10.1074/jbc.RA119.012377

54. Whicher J.R., Mackinnon R (2016) **Structure of the voltage-gated K+ channel Eag1 reveals an alternative voltage sensing mechanism** *Science* **353**:664–669 https://doi.org/10.1126/science.aaf8070

55. Whicher J.R., Mackinnon R (2019) **Regulation of Eag1 gating by its intracellular domains** *Elife* **8** https://doi.org/10.7554/eLife.49188

56. Wynia-Smith S.L., Gillian-Daniel A.L., Satyshur K.A., Robertson G.A (2008) **hERG gating microdomains defined by S6 mutagenesis and molecular modeling** *J Gen Physiol* **132**:507–520 https://doi.org/10.1085/jgp.200810083

57. Zhao Y., Goldschen-Ohm M.P., Morais-Cabral J.H., Chanda B., Robertson G.A (2017) **The intrinsically liganded cyclic nucleotide–binding homology domain promotes KCNH channel activation** *The Journal of General Physiology* https://doi.org/10.1085/jgp.201611701

58. Ziechner U., Schönherr R., Born A.-K., Gavrilova-Ruch O., Glaser R.W., Malesevic M., Küllertz G., Heinemann S.H (2006) **Inhibition of human ether à go-go potassium channels by Ca2+/calmodulin binding to the cytosolic N- and C-termini** *FEBS Journal* **273**:1074–1086 https://doi.org/10.1111/j.1742-4658.2006.05134.x

Author information

Reham Abdelaziz
Oncophysiology Group. Max Planck Institute for Multidisciplinary Sciences, City Campus

Adam P. Tomczak
Oncophysiology Group. Max Planck Institute for Multidisciplinary Sciences, City Campus

Andreas Neef
Neurophysics Laboratory. Göttingen Campus Institute for Dynamics of Biological Networks
ORCID iD: 0000-0003-4445-7478

Luis A. Pardo
Oncophysiology Group. Max Planck Institute for Multidisciplinary Sciences, City Campus
For correspondence: pardo@mpinat.mpg.de
ORCID iD: 0000-0003-1375-4349

Editors

Reviewing Editor
Andres Jara-Oseguera
The University of Texas at Austin, United States of America

Senior Editor
Kenton Swartz
National Institute of Neurological Disorders and Stroke, National Institutes of Health, United States of America

Reviewer #1 (Public Review):

Gating of Kv10 channels is unique because it involves coupling between non-domain swapped voltage-sensing domains, a domain-swapped cytoplasmic ring assembly formed by the N- and C-termini, and the pore domain. Recent structural data suggests that activation of the voltage sensing domain relieves a steric hindrance to pore opening, but the contribution of the cytoplasmic domain to gating is still not well understood. This aspect is of particular importance because proteins like Calmodulin interact with the cytoplasmic domain to regulate channel activity. The effects of Calmodulin (CaM) in WT and mutant channels with disrupted cytoplasmic gating ring assemblies are contradictory, resulting in inhibition or activation, respectively. The underlying mechanism for these discrepancies is not understood. In the present manuscript, Reham Abdelaziz and collaborators use electrophysiology, biochemistry, and mathematical modeling to explore the mechanistic effects on gating of various mutations and deletions that disrupt inter-subunit interactions at the cytoplasmic gating ring assembly and the consequences for channel modulation by CaM. From the beginning, it becomes challenging for non-experts to grasp the structural basis of the perturbations that are introduced (ΔPASCap and E600R), because no structural data or schematic cartoons are provided to illustrate the rationale for those deletions or their potential mechanistic effects. In addition, the lack of additional structural information or illustrations, and a somewhat confusing discussion of the structural data, make it challenging for a reader to reconcile the experimental data and mathematical model with a particular structural mechanism for gating, limiting the impact of the work.

By expressing mutants in oocytes and recording currents using Two Electrode Voltage-Clamp (TEV), it is found that both ΔPASCap and E600R mutants have biphasic voltage-activation curves, with two clear components contributing to activation and deactivation kinetics. Notably, the first component involving activation occurs at voltages where WT channels are mostly closed. Larger deletions at the N-terminus that further disrupt the cytoplasmic gating ring assembly accentuate the first component by heavily disfavoring the second one. The data can be well described by three components involving a closed state and two open states O1 and O2, in which the second component O2 is the one affected by the mutations and deletions. Based on the structural data, the first component is hypothesized to be associated with voltage sensor activation, whereas the second component is associated with conformational changes at the cytoplasmic ring. Consistent with this interpretation, a deletion construct where the covalent link between the voltage sensor and pore has been severed is shown to primarily affect that first component. Also consistent with the first component involving voltage-sensor activation, it is found that divalent cations that are known to stabilize the voltage sensor in its most deactivated conformations, shift the occupancy of the first component to more depolarizing potentials. Activation towards and closure from the first component is slow, whereas channels close rapidly from O2. A rapid alternating pulse protocol is used to take advantage of the difference in activation and deactivation kinetics between the two open components in the mutants and thus drive an increasing number of channels toward state O1. Currents activated by the alternating protocol reached larger amplitudes than those elicited by a long depolarization to the same voltage. This finding is interpreted as an indication that the first component (O1) has a larger conductance than the second (O2). It is shown that conditioning pulses to very negative voltages results in currents that are larger and activate more slowly than those elicited at the same voltage but starting from less negative conditioning pulses. In voltage-activated curves, the component corresponding to state O1 is shown to be favored by increasingly negative conditioning voltages as compared to less negative ones. This is interpreted as indicating that the first open component O1 is primarily accessed from so-called 'deeply closed' states in which voltage sensors are in their most deactivated position(s). Consistently, a mutation that destabilizes these deactivated states is shown to largely suppress the first component in voltage-activation curves for both ΔPASCap and E600R channels. It is also shown that

stimulating calcium entry into the oocytes with ionomycin and thapsigargin, which is assumed to enhance CaM-dependent modulation, results in preferential potentiation of the first component in ΔPASCap and E600R, and this potentiation is attenuated by including an additional mutation that disfavors deeply closed states where voltage sensors are (mostly) deactivated. Together, these results are interpreted as an indication that calcium-CaM preferentially stabilizes O1 in mutant channels, thus favoring activation, whereas in WT channels lacking occupancy of O1, CaM stabilizes closed states and is therefore inhibitory. Moreover, it is found that the potentiation of ΔPASCap and E600R by CaM is more strongly attenuated by mutations in the channel that disrupt interaction with the C-terminal lobe of CaM than mutations affecting interaction with the N-terminal lobe. Finally, a mathematical model is proposed consisting of two layers involving two activation steps for the voltage sensor, and one conformational change in the cytoplasmic gating ring - completion of both sets of conformational changes is required to access state O2, but accessing state O1 only requires completion of the first voltage-sensor activation step in the four subunits. The model qualitatively reproduces most major findings on the mutants.

There are several concerns associated with the analysis and interpretations that are provided. First, the conductance-voltage (G-V) relations for the mutants do not seem to saturate, and the absolute open probability is not quantified for any mutant under any condition. This makes it impossible to quantitatively compare the relative amplitudes of the two components because the amplitude of the second component remains undetermined. This makes it challenging to interpret results involving perturbations that affect the relative occupancy of O1 and O2, such as those in Figures 2, 6, and 7, and also raises concerns about the extent to which model parameters can be constrained. This issue is made even more serious by the observation that the currents in both key mutants (ΔPASCap and E600R) are extremely slow and do not appear to reach steady-state over the intervals that are studied. This reduces confidence in the parameters associated with G-V relations, as the shape and position of both components might change significantly if longer pulses were used. This is not addressed or acknowledged in the manuscript. Further, because the mutant channel currents do not saturate at the most positive potentials and time intervals examined, the kinetic characterization based on reaching 80% of the maximum seems inappropriate, because the 100% mark is arbitrary. Further, the kinetics for some of the other examined mutants (e.g. those in Fig. 2A) are not shown, making it difficult to assess the extent to which the data could be affected by having been measured before full equilibration. There are additional aspects associated with gating kinetics that are not appropriately explored. For example, I would expect that the enhanced current amplitudes from Figure 5 are only transient, ultimately reaching a smaller steady-state current magnitude that depends only on the stimulation voltage and is independent of the pre-pulse. The entire time course including the rise-time and decay is not examined experimentally. This raises concern on whether occupancy of state O1 might be overestimated under some experimental conditions if a fraction of the occupancy is only transient. The mathematical model is not utilized to examine some of these slower relaxations - this may be because the model does not reproduce these slow processes, which would represent a serious shortcoming given that the slow kinetics appear to be intrinsic to transitions around state O1. The significance of the results with the Δ2-10.L341Split is unclear. First, structural as well as functional data has established that the coupling of the voltage sensor and pore does not entirely rely on the S4-S5 linker, and thus the Split construct could still retain coupling through other mechanisms, which is consistent with the prominent voltage dependence that is observed. If both state O1 and O2 require voltage sensor activation, it is unclear why the Split construct would affect state O1 primarily, as suggested in the manuscript, as opposed to decreasing occupancy of both open states.

The figure legends and text do not describe which solutions exactly were utilized for each experiment, and the rationale for choosing some solutions over others is not properly explained. The reversal potential for solutions used to measure voltage-activation curves falls right at the spot where occupancy of the first component peaks (e.g. see Figure 1B). Because

no zero-current levels are shown on the current traces, it becomes very hard to determine which voltages correspond to each of the currents (see Fig. 1A). It is unclear whether any artifacts could have been introduced to the mutant activation curves at voltages close to the reversal potential. One key assumption that is not well-supported by the data pertains to the difference in single-channel conductance between states O1 and O2 - no analysis or discussion is provided on whether the data could also be well described by an alternative model in which O1 and O2 have the same conductance. No additional experimental evidence is provided related to the difference in conductance, which represents a key aspect of the mathematical model utilized to interpret the data. The CaM experiments are potentially very interesting and could have wide physiological relevance. However, the approach utilized to activate CaM is indirect and could result in additional non-specific effects on the oocytes that could affect the results.

The description of the mathematical model that is provided is difficult to follow, and some key aspects are left unclear, such as the precise states from which state O1 can be accessed, and whether there is any direct connectivity between states O1 and O2 - different portions of the text appear to give contradictory information regarding these points. Several rate constants other than those explicitly mentioned to represent voltage sensor activation are also assigned a voltage dependence - the mechanistic basis of that voltage dependence is unclear. Finally, a clear mechanistic explanation for the full range of effects that the ΔPASCap and E600R mutants have on channel function is lacking, as well as a detailed description of how those newly uncovered transitions would influence the activity of the WT channel; this latter point is important when considering whether the findings in the manuscript advance our understanding of the gating mechanism of Kv10 channels in general, or are specific to the particular mutants that are studied. It is unclear, for example, how both the mutation or the deletion at the cytoplasmic gating ring enable conduction by state O1, especially when considering the hypothesis put forward in this study that transition to O1 exclusively involves transitions by the voltage sensor and not the cytoplasmic gating ring. It is also not clearly described whether a non-conducting state with the equivalent state-connectivity as O1 can be accessed in WT channels, or if a state like O1 can only be accessed in the mutant channels. Importantly, if a non-conducting state with the same connectivity to O1 were to be accessed in WT channels, it would be expected that an alternating pulse protocol as in Fig. 4 would result in progressively decreasing currents as the occupancy of the non-conducting state equivalent to O1 is increased. Because this is not the case, it means that mutation and deletion cause additional perturbations on the gating energetics relative to WT, which are not clearly fleshed out.

Reviewer #2 (Public Review):

Summary:
The EAG family of ion channels is associated with many pathological conditions and are considered a target for the treatment of disease such as cancer. In this study, Abdelaziz et. al. examine the role of interaction between PAS domain and CNBHD in voltage-dependent gating of EAG channels. Based on their data, the authors conclude that they have identified a hidden open state that is only accessible in the mutant channels but not in the wild type. This hidden open state O1 can distinguished from the canonical open state O2 because it exhibits very different voltage-dependence. Although it is clear that the kinetics of these two open states are different, I have concerns about whether the data presented in this manuscript rule out alternate explanations. The idea that PAS domain deletions uncover a hidden open state is an extraordinary claim and if established, it has the potential to open a completely new approach to studying early gating transitions of these channels.

Strengths:
1. The study has identified a number of potentially interesting mutants that modulate voltage-dependent gating.

2. The discovery of a hidden open state due to mutations in the cytosolic domains is quite astonishing.

Weaknesses:
1. WT EAG currents are far right shifted compared to previously published data. It is not clear whether it is the recording conditions but at 0 mV very few channels are open. Compare this with recordings reported previously of the same channel hEAG1 by Gail Robertson's lab (Zhao et. al. (2017) JGP). In that case, most of the channels are open at 0 mV. There must be at least 25 mV shift in voltage-dependence. These differences are unusually large.

2. In most of the mutants, O2 state becomes more prevalent at potentials above +50 mV. At these potentials, endogenous voltage-dependent currents are often observed in xenopus oocytes. The observed differences between the various mutants might simply be a function of the expression level of the channel versus endogenous currents.

3. Voltage-dependence of the kinetics of WT currents appears a bit strange. Why is the voltage-dependence saturated at 0 mV even though very few channels have activated at that point? I cannot imagine any kinetic model that can lead to such unusual voltage-dependence of kinetics.

4. One of the other concerns I have is that in many cases, it is clear that the pulse is too short to measure steady-state voltage-dependence. For instance, the currents in -160 mV and -100 mV in Figure 6A and 6B are not saturated.

Reviewer #3 (Public Review):

Summary:
The present manuscript by Reham Abdelaziz and colleagues addresses the gating of Kv10.1, which belongs to the KCNH gene family and contains other subfamilies such as Kv11 (ERG) and Kv12 (ELK). They all have fundamental physiological roles, from cardiac repolarization to modulation of neuronal excitability and cancer physiology. They have a non-domain swapped architecture at the molecular level; both voltage and Ca-CaM modulate the channel function. They contain an intracellular gating ring formed by a PAS domain (in the N-term) that interacts intimately with the cNBHD (C-term) of the neighbor subunit but also with the cytosolic part of the voltage sensor domain and the C-linker. Mutations in the N- or C-terminus modify the gating dramatically. This complex network of interactions makes the cytosolic section and the PAS domain in particular, an alluring part of the channel to study as responsible for the coupling between the movements of the voltage sensor and the gating ring.

In this paper, Reham Abdelaziz and colleagues address a fundamental question of how in the Kv10.1 channels, the movement of the voltage sensor is coupled to the intracellular gating ring rotation to make the channel conduct ions. The authors perform a series of deletions and mutations in the N-terminal section of the channel (PAS domain) and in the C-terminus (cNHBD) and observe a biphasic behavior on the modified EAG channels that they interpret as two populations of open states, one of them not visible in the WT and only available because of the mutations introduced. While this is a fascinating hypothesis and it fits with the depolarizing range of potentials of the WT channels, there are some issues that, if addressed, will make this work very valuable for biophysicists and molecular physiologists interested in voltage-gated ion channels.

Strengths:
The work presented addresses one of this channel's most fascinating and challenging features in the KCNH family. The authors use adequate mutations and electrophysiological techniques to address the questions they are trying to answer. They help them explore the behavior of the channels and build a Markov model to understand the underlying mechanism.

Weaknesses:
Although very well established, the experimental conditions used in the present manuscript introduce uncertainties, weakening their conclusions and complicating the interpretation of the results. The authors performed most of their functional studies in Cl-based solutions that can become a non-trivial issue when the range of voltages explored extends to very depolarizing potentials such as +120mV. Oocytes endogenously express Ca2+-activated Cl- channels that will rectify Cl- at very depolarizing potentials -due to an increase in the driving force- and contribute dramatically to the current's amplitude observed at the test pulse in the voltage ranges where the authors identify the second open state.

The authors propose a two-layer Markov model with two open states approximating their results. However, the results obtained with the mutants suggest an inactivated state accessible from closed states and a change in the equilibrium between the close/inactivated/open states that could also explain the observed results; therefore, other models could approximate their data.

That said, if the results obtained by the authors get confirmed under different experimental conditions in the absence of Cl-, this present work could be instrumental in understanding the gating mechanisms of the KCNH family.

Author Response

We thank the reviewers and editors for their deep, thoughtful and constructive assessment of our manuscript. We nevertheless would like to reply to the Reviewers reports.

> ### *Reviewer #1.*
>
> *(...) The data can be well described by three components involving a closed state and two open states O1 and O2, in which the second component O2 is the one affected by the mutations and deletions*

This statement is not completely clear to us. What we propose is that O1 is not visible in WT, only in the mutants. What would be affected is the access to O1 and the transition between O1 and O2, but not O2 itself.

> *From the beginning, it becomes challenging for non-experts to grasp the structural basis of the perturbations that are introduced (ΔPASCap and E600R), because no structural data or schematic cartoons are provided to illustrate the rationale for those deletions or their potential mechanistic effects. In addition, the lack of additional structural information or illustrations, and a somewhat confusing discussion of the structural data, make it challenging for a reader to reconcile the experimental data and mathematical model with a particular structural mechanism for gating, limiting the impact of the work.*

Thank you very much for pointing this out and our apologies for the missing cartoon. It will be provided in the revised version.

> *There are several concerns associated with the analysis and interpretations that are provided. First, the conductance-voltage (G-V) relations for the mutants do not seem to saturate, and the absolute open probability is not quantified for any mutant under any condition. This makes it impossible to quantitatively compare the relative amplitudes of the two components because the amplitude of the second component remains undetermined. [...] This reduces confidence in the parameters associated with G-V*

> *relations, as the shape and position of both components might change significantly if longer pulses were used.*

We agree that the endpoint of activation is ill-defined in the cases where a steady-state is not reached. This does indeed hamper quantitative statements about the relative amplitude of the two components. However, while the overall shape does change, its position (voltage dependence) would not be affected by this shortcoming. The data therefore supports the claim of the "existence of mutant-specific O1 and its equal voltage dependence across mutants."

> *Further, because the mutant channel currents do not saturate at the most positive potentials and time intervals examined, the kinetic characterization based on reaching 80% of the maximum seems inappropriate, because the 100% mark is arbitrary.*

We agree that the assessment of kinetics by a t80% is not ideal. We originally refrained from exponential fits because they introduce other issues when used for processes that are not truly exponential (as is the case here). To address the concerns, we will add time constants from these fits in the revised version. Please note that in Figure 3, we do provide time constants, and they support the statement made.

> *Further, the kinetics for some of the other examined mutants (e.g. those in Fig. 2A) are not shown, making it difficult to assess the extent to which the data could be affected by having been measured before full equilibration.*

This seems to be a misunderstanding. Δ2-10 kinetics is shown in Fig. 2c. Δ-eag is shown in Fig. 3. We will make sure to state this explicitly in the revised version.

> *For example, I would expect that the enhanced current amplitudes from Figure 5 are only transient, ultimately reaching a smaller steady-state current magnitude that depends only on the stimulation voltage and is independent of the pre-pulse. The entire time course including the rise-time and decay is not examined experimentally. This raises concern on whether occupancy of state O1 might be overestimated under some experimental conditions if a fraction of the occupancy is only transient. The mathematical model is not utilized to examine some of these slower relaxations - this may be because the model does not reproduce these slow processes, which would represent a serious shortcoming given that the slow kinetics appear to be intrinsic to transitions around state O1.*

Thank you for thinking so deeply about the problem. We identified the same questions and did explore them using the model (Figure 8 c). Your intuition is confirmed there, the slow kinetics leads to a decrease of O1 occupancy after a transient accumulation. We intend to study this experimentally as well in the revised version.

> *The significance of the results with the Δ2-10.L341Split is unclear. First, structural as well as functional data has established that the coupling of the voltage sensor and pore does not entirely rely on the S4-S5 linker, and thus the Split construct could still retain coupling through other mechanisms, which is consistent with the prominent voltage dependence that is observed. If both state O1 and O2 require voltage sensor activation, it is unclear why the Split construct would affect state O1 primarily, as suggested in the manuscript, as opposed to decreasing occupancy of both open states.*

Thank you for pointing out the unclear nature of our arguments. We rephrase in the following and will do so in the revised document: If, in non-split mutants, the upward transition of S4 allows entry to O1, it is reasonable to assume that the movement is not

transmitted the same way in the split and the transition into O1 is less probable. The observation that, in the split, entry into O1 requires higher depolarization and appears to be less likely, suggests that downstream of S4 (beyond position 342), there is a mechanism to convey S4 motion to the gate of the mutants.

> *The figure legends and text do not describe which solutions exactly were utilized for each experiment, […] Because no zero-current levels are shown on the current traces, it becomes very hard to determine which voltages correspond to each of the currents (see Fig. 1A).*

Will be corrected.

> *… the rationale for choosing some solutions over others is not properly explained. […] The reversal potential for solutions used to measure voltage-activation curves falls right at the spot where occupancy of the first component peaks (e.g. see Figure 1B). […] It is unclear whether any artifacts could have been introduced to the mutant activation curves at voltages close to the reversal potential.*

The high potassium extracellular solution was chosen to obtain tail currents of sufficient size, warranting precise determination of the reversal potential for every individual experiment. In this way, we ensured that there were no artifacts introduced to the activation curves. Tail currents were used when closing was reasonably fast (ΔPASCapL322H and E600RL322H), but otherwise, we used the amplitude at the end of the pulse to get the reversal potential.

> *One key assumption that is not well-supported by the data pertains to the difference in single-channel conductance between states O1 and O2 - no analysis or discussion is provided on whether the data could also be well described by an alternative model in which O1 and O2 have the same conductance. No additional experimental evidence is provided related to the difference in conductance, which represents a key aspect of the mathematical model utilized to interpret the data.*

We agree that the relative conductance of O1 and O2 is a key point. Our proposal mainly stems from the data presented in Fig. 4 and the amplitudes of the two components of the tail at potentials where both states are visible. We also agree that whole cell currents represent a product of occupancy and conductance and that only single channel recordings can produce unambiguous proof for the higher conductance of O1. We have embarked on a series of experiments directly addressing this in the mutants that will be reported in the revised version. Still, we did explore this issue with the model. Following the path of the least number of assumptions, we initially tested models with equal conductance for both states. None of these models was able to reproduce the shape of the tails and the prepulse-dependent increase.

> *The CaM experiments are potentially very interesting and could have wide physiological relevance. However, the approach utilized to activate CaM is indirect and could result in additional non-specific effects on the oocytes that could affect the results.*

Thank you for the appreciative comments about the relevance of our results. We are aware of the potential side effects of the use of thapsigargin and ionomycin, but we still used this approach as an established method to raise intracellular Ca2+. This said, we would like to point out that the effects of Ca2+ increase on channel behavior do revert with a time course that mirrors the estimated time course of Ca2+ itself (supplement 1 to figure 7), suggesting that we are monitoring a Ca2+-dependent event.

> *The description of the mathematical model that is provided is difficult to follow, and some key aspects are left unclear, such as the precise states from which state O1 can be accessed, and whether there is any direct connectivity between states O1 and O2 - different portions of the text appear to give contradictory information regarding these points.*

This seems to be a misunderstanding: supplement 1 to figure 8 graphically details the model's layout and explicitly shows the connections to the two open states. It also shows that these are not connected. We will make sure that the text is more clearly stating this fact. We did explore models with one open state connected to more than one other state (loops) and found that none of these models can reproduce the large range of depolarizations for with conductance is reduced as compared to lower and higher depolarization (Figure 1).

> *Several rate constants other than those explicitly mentioned to represent voltage sensor activation are also assigned a voltage dependence - the mechanistic basis of that voltage dependence is unclear.*

Some fundamental properties we observed in the mutants can be explained with constant, voltage-independent rate constants into and out of both open states. Specifically, it was possible to achieve behavior very close to that displayed in Figure 8c with constant η, θ, ε, and ζ. We then attempted to also reproduce the strong prepulse-dependence (Figure 6A and B) and found that we needed additional degrees of freedom to incorporate both behaviors with one parameter set. We could either add more states, and thereby rates, or introduce voltage dependence to η and θ. With already 32 states and 10 rates, we decided to adopt the less complex model variant. We agree that this probably reduced the interpretability of the model. As a rule, a transition with a voltage-dependence of the functional form of Eq.1 corresponds to the kinetic properties of two or three transitions, where one is voltage-independent (setting the maximal rate) and one has the classical exponential shape expected from truly molecular transitions.

We also agree that, conceptually, the transitions between the two layers – tentatively associated with a transition in the ring structure– should be voltage-independent. Interestingly, their voltage dependence is very similar to the voltage dependence of the early activation, i.e. centered at -100 and -120mV, similar to β. We therefore attempted to replace the voltage dependence of κ and λ with a state-dependence. To this end, we introduced a parameter that modified κ and λ depending on the state's position along the α-β axis. While it seemed possible to include all desired features in a model with state-dependent κ and λ, it proved extremely difficult to tune the parameters. Eventually, we reverted to purely voltage-dependent and not state-dependent transition rates κ and λ. Nevertheless, we believe that their voltage dependence could be replaced by some form of state-dependence, i.e. by rates κ and λ that change systematically from the left-hand side of the scheme to its right-hand side.

> *Finally, a clear mechanistic explanation for the full range of effects that the ΔPASCap and E600R mutants have on channel function is lacking, as well as a detailed description of how those newly uncovered transitions would influence the activity of the WT channel.*

We agree. Ultimate mechanistic explanations will have to await data from protein structures of intermediate states and in particular the mutant-specific open state.

> *…as well as a detailed description of how those newly uncovered transitions would influence the activity of the WT channel; this latter point is important when considering whether the findings in the manuscript advance our understanding of the gating*

mechanism of Kv10 channels in general, or are specific to the particular mutants that are studied.

We still do not know if the transitions to O1 are identical in the mutants and WT, although our data opens the path to dissecting the interplay of intracellular domains and voltage sensor. We think that the results are relevant for KCNH channels in general because we have made visible otherwise invisible states.

It is unclear, for example, how both the mutation or the deletion at the cytoplasmic gating ring enable conduction by state O1, especially when considering the hypothesis put forward in this study that transition to O1 exclusively involves transitions by the voltage sensor and not the cytoplasmic gating ring.

The transition to O1 is in our model made possible by a displacement of the voltage sensor. In our view, when this occurs with a properly folded and positioned intracellular ring, permeation (access to O1) is precluded. It is precisely the distortion in the intracellular ring induced by mutation or deletion what allows access to O1.

It is also not clearly described whether a non-conducting state with the equivalent state-connectivity as O1 can be accessed in WT channels, or if a state like O1 can only be accessed in the mutant channels. Importantly, if a non-conducting state with the same connectivity to O1 were to be accessed in WT channels, it would be expected that an alternating pulse protocol as in Fig. 4 would result in progressively decreasing currents as the occupancy of the non-conducting state equivalent to O1 is increased. Because this is not the case, it means that mutation and deletion cause additional perturbations on the gating energetics relative to WT, which are not clearly fleshed out.

Thank you for highlighting this important question. Following the arguments in the answer to the previous comment, our experiments cannot provide proof for the existence or accessibility of O1 in WT channels. We favor the interpretation that it is not accessible, because, as you point out, this is supported by the outcome of the alternating pulse on WT (figure 4A) and the paradoxical effect of CaM activation. However, this interpretation hinges on the hypothesis that the kinetics of entry into and departure from O1 would be the same in WT channels, as it is in the mutants. Because transitions into a non-conducting O1 would be only indirectly observable in the WT channel, this assumption would be extremely difficult to test.

Reviewer #2.

WT EAG currents are far right shifted compared to previously published data. It is not clear whether it is the recording conditions but at 0 mV very few channels are open. Compare this with recordings reported previously of the same channel hEAG1 by Gail Robertson's lab (Zhao et. al. (2017) JGP). In that case, most of the channels are open at 0 mV. There must be at least 25 mV shift in voltage-dependence. These differences are unusually large.

G-V curves presented in the literature show a large variability. Depending on the conditions, reported V1/2 values in Xenopus oocytes range from -43 mV (Schönherr et al., 2002 DOI: 10.1016/s0014-5793(02)02365-7) to +16 mV (Lörinczi et al, 2015 DOI: 10.1038/ncomms7672) through +4.1 mV (Lörinczi et al., 2016 DOI: 10.1074/jbc.M116.733576), or +10 mV (in the IUPHAR database). The results in the current manuscript are not significantly different from our previously published results on WT channels. In the report the reviewer is referring to, one source of the difference could be that Zhao et al. had no independent information about the reversal potential. In our experiments, we used solutions with high [K]ext. This places the

reversal potential in a voltage range within measurable eag currents and thus allows direct determination of the reversal potential, together with the slow kinetics of the tails and the negative shift in the activation. We would argue that this makes the G-V curves less prone to assumptions, albeit for the price of large error bars around the reversal potential. Additionally, the presence of Mg2+ in the extracellular solutions can change the apparent V1/2 depending on the stimulation protocol.

> *In most of the mutants, O2 state becomes more prevalent at potentials above +50 mV. At these potentials, endogenous voltage-dependent currents are often observed in xenopus oocytes. The observed differences between the various mutants might simply be a function of the expression level of the channel versus endogenous currents.*

Because we were aware of the potential issue of endogenous chloride currents in oocytes, we included data recorded in chloride-free solutions. Those show comparable results, and thus we conclude that endogenous currents are not the origin of the differences between mutants. We will clarify which solutions were used in the figure legends of the revised version and also include the argument against sizable endogenous current contributions in the revision. In a separate line of experiments, we expressed some of the mutants in HEK cells. Despite small current amplitudes, we were able to replicate the findings of two components, providing oocyte-independent evidence for the existence of a second open state.

> *Voltage-dependence of the kinetics of WT currents appears a bit strange. Why is the voltage-dependence saturated at 0 mV even though very few channels have activated at that point? I cannot imagine any kinetic model that can lead to such unusual voltage-dependence of kinetics.*

The fact that voltage dependence of open probability and voltage dependence of activation time constant do not align reflects the multi-state nature of the underlying gating scheme. More than one of several sequential transitions limit the overall kinetics. In this case, the apparent kinetics can reflect a different “bottleneck” transition at different voltage ranges.

> *One of the other concerns I have is that in many cases, it is clear that the pulse is too short to measure steady-state voltage-dependence. For instance, the currents in -160 mV and -100 mV in Figure 6A and 6B are not saturated.*

While we agree that steady-state curves can simplify quantitative evaluation – especially the normalization applied in the I/Imax curves in figure 6 – the conclusion of two components is independent of the absolute amplitude under steady state. The fact that in the raw current traces in Figure 6A, after a -160V prepulse, the same current amplitude is reached for two depolarizations (60 and 90 mV) but not for the intermediate depolarization, can only be explained by an I-V curve that has a minimum. Therefore, the raw data directly support the evidence of finding two components, even if the subsequent analysis is affected by insufficient test pulse durations.

Reviewer #3

Although very well established, the experimental conditions used in the present manuscript introduce uncertainties, weakening their conclusions and complicating the interpretation of the results. The authors performed most of their functional studies in Cl-based solutions that can become a non-trivial issue when the range of voltages explored extends to very depolarizing potentials such as +120mV. Oocytes endogenously express Ca2+-activated Cl- channels that will rectify Cl- at very depolarizing potentials -due to an increase in the driving force- and contribute dramatically to the current's amplitude

> *observed at the test pulse in the voltage ranges where the authors identify the second open state.*

As stated above, because we were aware of the potential issue of endogenous chloride currents in oocytes, we performed many of the experiments in chloride-free solutions. We conclude that endogenous currents are not the origin of the differences between mutants because the results were comparable regardless of the presence of chloride. We will clarify which solutions were used in the figure legends of the revised version and also include the argument against sizable endogenous current contributions in the revision. In a separate line of experiments, we expressed some of the mutants in HEK cells. Despite small current amplitudes, we were able to replicate the findings of two components, providing oocyte-independent evidence for the existence of a second open state.

> *The authors propose a two-layer Markov model with two open states approximating their results. However, the results obtained with the mutants suggest an inactivated state accessible from closed states and a change in the equilibrium between the close/inactivated/open states that could also explain the observed results; therefore, other models could approximate their data.*

In the process of model development, we tested a large number of configurations. Those included models with a single open state which we connected to two closed (or inactivated) states that were not directly connected to each other and populated at different voltage ranges. In doing so, we attempted to allow access to the single open state from different regions of the "state-space", reflecting the two voltage ranges of high conductance. However, in our hands, such a "loop" in the state-space inadvertently leads to a weak separation of the two states and a weak effect of prepulse potentials. The underlying reason is that given the short activation and deactivation time constants, a single open state in a loop provides an effective short-cut, linking otherwise separated parts of the state-space. To achieve the clear separation of the two component's voltage dependence, two open states that are not connected to each other were essential. As we wrote in response to other comments above, the ultimate proof of two different open states cannot come from modeling, but from single channel measurements.